DNA 2753F

GULF RADIATION TECHNOLOGY

Gulf-RT-A10767

ELECTRONIC AND IONIC REACTIONS IN ATMOSPHERIC GASES

Yearly Technical Summary Report
September 1, 1970, through June 30, 1971

by

R. H. Neynaber, J. A. Rutherford, and D. A. Vroom

Prepared for
Defence Nuclear Agency
under
Contract DASA01-69-C-0044

July 28, 1971

GULF RADIATION TECHNOLOGY
A DIVISION OF GULF ENERGY & ENVIRONMENTAL SYSTEMS COMPANY
P.O BOX 608, SAN DIEGO, CALIFORNIA 92112

UNCLASSIFIED

Security Classification

DOCUMENT CONTROL DATA - R & D

(Security classification of title, body of abstract and indexing annotation must be entered when the overall report is classified)

1. ORIGINATING ACTIVITY (Corporate author) Gulf Radiation Technology P. O. Box 608 San Diego, California 92112	2a. REPORT SECURITY CLASSIFICATION UNCLASSIFIED 2b. GROUP

3. REPORT TITLE

Electronic and Ionic Reactions in Atmospheric Gases

4. DESCRIPTIVE NOTES (Type of report and inclusive dates)

Yearly Summary Report - September 1, 1970 through June 30, 1971

5. AUTHOR(S) (First name, middle initial, last name)

R. H. Neynaber - J. A. Rutherford - D. A. Vroom

6. REPORT DATE	7a. TOTAL NO. OF PAGES	7b. NO. OF REFS
July 1971	102	26

8a. CONTRACT OR GRANT NO. DASA 01-69-C-0044 b. PROJECT NO. NWER XAXH c. Task and Subtask D010 d. Work Unit 01	9a. ORIGINATOR'S REPORT NUMBER(S) Gulf-RT-A10767 9b. OTHER REPORT NO(S) (Any other numbers that may be assigned this report) DNA 2753F

10. DISTRIBUTION STATEMENT

Approved for public release; distribution unlimited.

11. SUPPLEMENTARY NOTES	12. SPONSORING MILITARY ACTIVITY
	Director Defense Nuclear Agency Washington, D. C. 20305

13. ABSTRACT

Laboratory measurements indicate that the metastable ions of O^+ in reaction with N_2 in the low-energy range (14 eV) react to form principally N_2^+, while the ion molecule reaction to form NO^+ has a very small probability. The ground-state O^+ reacts mainly to form NO^+. The abundance of metastable $O^{+2}D$ ions was determined using the observation that $O^{+2}D + N_2$ has a small cross section for forming NO^+. The ion-energy dependences for both reactions were measured within the energy range 1.0 to 500 eV.

DD FORM 1 NOV 68 1473

UNCLASSIFIED

Security Classification

14 KEY WORDS	LINK A		LINK B		LINK C	
	ROLE	WT	ROLE	WT	ROLE	WT
Atmospheric Chemistry						
Ionic Reactions						
Excited State Chemistry						

DNA 2753F

GULF RADIATION TECHNOLOGY

Gulf-RT-A10757

ELECTRONIC AND IONIC REACTIONS IN ATMOSPHERIC GASES

Yearly Technical Summary Report
September 1, 1970 through June 30, 1971

This work was supported by the
Defense Nuclear Agency
under NWER Subtask HD-010-01

Work done by:

A. E. Kristensen
J. K. Layton
R. H. Neynaber
J. A. Rutherford
D. A. Vroom

Report written by:

R. H. Neynaber
J. A. Rutherford
D. A. Vroom

Approved for public release; distribution unlimited.

Gulf Radiation Technology
Project 6103

July 28, 1971

GULF RADIATION TECHNOLOGY
A DIVISION OF GULF ENERGY & ENVIRONMENTAL SYSTEMS COMPANY
P.O. BOX 608, SAN DIEGO, CALIFORNIA 92112

ABSTRACT

Laboratory measurements indicate that the metastable ions of O^+ in reaction with N_2 in the low-energy range (14 eV) react to form principally N_2^+, while the ion molecule reaction to form NO^+ has a very small probability. The ground-state O^+ reacts mainly to form NO^+. The abundance of metastable $O^{+2}D$ ions was determined using the observation that $O^{+2}D + N_2$ has a small cross section for forming NO^+. The ion-energy dependences for both reactions were measured within the energy range 1.0 to 500 eV.

CONTENTS

TABLES

Tables (Cont.)

FIGURES

Figures (Cont.)

1. INTRODUCTION

The ability to transmit radio and radar signals through the atmosphere is strongly dependent on the free electron density in the ionosphere. The density of these free electrons is a function of both the amount of ionization that is occurring and the magnitude of the rate coefficients for the various mechanisms available for electron loss. In the normal atmosphere, ionization is produced primarily by photoionization processes initiated by solar radiation. During periods of increased solar activity, the amount of ionization and, hence, the free electron density are increased. These increases result in degradation of radio and radar equipment performance.

Artificial disturbances of the ionosphere, such as those resulting from nuclear weapons detonation, considerably increase the free electron density. The resultant loss in radio and radar performance can seriously affect the operation of military communications systems. Since the Nuclear Test Ban Treaty has eliminated atmospheric testing of nuclear weapons, it is not possible to ascertain the degree to which artificial disturbances of this nature will influence electromagnetic transmission. Therefore, considerable effort has been expended on laboratory and theoretical studies of atmospheric ionization that would be expected from detonating weapons, and on the deionization processes that tend to return the atmosphere to its normal condition.

Part of the overall interest in the upper atmospheric process is reflected in the Defense Nuclear Agency (DNA) Reaction Rate Program. This program, which supports research in the study of atmospheric deionization, involves <u>in situ</u> measurements of natural disturbances in the atmosphere

(e. g., Polar Cap Absorption Events), theoretical studies and laboratory measurements of pertinent reaction rates, cross sections, and other features of the interactions that may occur among electrons, ions, and neutral species present in the upper atomsphere. Current progress in the field is also monitored through the DNA Reaction Rate Handbook.[1] The program under way in our laboratory (DNA contract DASA01-69-C-0044) is concerned with one aspect of the deionization problem, namely, reactions of atmospheric ions and electrons with neutral species.

This ion-neutral reaction program is concerned primarily with the measurement of charge-transfer cross sections. Since the most probable means of losing electrons in the upper atmosphere is dissociative recombination, it is important to know the molecular ions present and their cross sections for formation. Much of the complexity of the ion-neutral chemistry of these processes arises because relatively minor constituents of the atmosphere are present. Many of these constituents have ionization potentials lower than the most dominant ionic species present in the atmosphere; thus, the chance of charge exchange between these minor species and the predominant ions is likely. In the past few years, researchers on the ion-neutral program under way at Gulf Radiation Technology (Rad Tech) have investigated reactions involving these minor constituents. This program has resulted in the measurement of charge-transfer cross sections between such atmospherically important ions as O^+, N^+, O_2^+, NO^+, N_2^+, and N_2O^+, and the neutral species H_2O, O_3, Na, Mg, and Ca. The results of these investigations have been reported in previous publications and Yearly Technical Summary Reports.[2-7] The reactions of minor constituents with ions of interest in the upper atmosphere have been extended this year to include reactions with iron. The experimental technique and the results obtained will be given in later sections of this report.

One aspect of ion-neutral reaction which is of great importance to an understanding of the overall problem, but which has received little attention

in the energy regime above thermal, is the effect of internal energy of the reactants on the cross section for a process and on the states of the products of the reactions. The major emphasis of the program this past year has been to investigate some of the more important reactions which occur in the upper atmosphere to see the effects of internal energy. Reactions of O^+, N_2^+, and N^+ with N_2, O_2, and NO have been studied. The techniques used to obtain excited reactant particles and the results obtained will be discussed in later sections.

2. EXPERIMENTAL

The crossed ion-modulated neutral-beam apparatus has been described previously.[2, 8, 9] The experiment reported here differs sufficiently, however, from past work to warrant a complete description of the machine and a discussion of the experimental procedure.

2.1 PRIMARY AND SECONDARY ION SYSTEMS

A schematic of the apparatus is shown in Fig. 1. The primary ions are extracted from an electron bombardment source and mass-analyzed at an energy of 75 eV in a 180° magnetic-mass spectrometer. After mass analysis, the ions pass through an aperture in an iron plate that shields the magnetic field of the mass analyzer from the succeeding regions of the apparatus. They are then retarded or accelerated to the desired collision energy, and pass through a field-free region before intersecting the neutral beam. Collimating apertures ensure that, from purely geometrical considerations, all primary ions pass through the modulated neutral beam (modulated at 100 Hz by mechanical chopping). Secondary ions resulting from collisions between the primary ions and neutrals are extracted along the direction of the primary ion beam by an electric field of approximately 2 V/cm. The ions then enter an electric field where their energy is increased to 1000 eV. Penetration of this accelerating field into the interaction region is reduced by use of a double grid structure. After acceleration, the ions pass through an electrostatic quadrupole lens[10] which forms the entrance slit for the 60° sector of the magnetic mass spectrometer. The selected ions impinge on the first dynode of a 14-stage CuBe electron multiplier. For all ions formed by charge transfer, the most abundant isotope was used

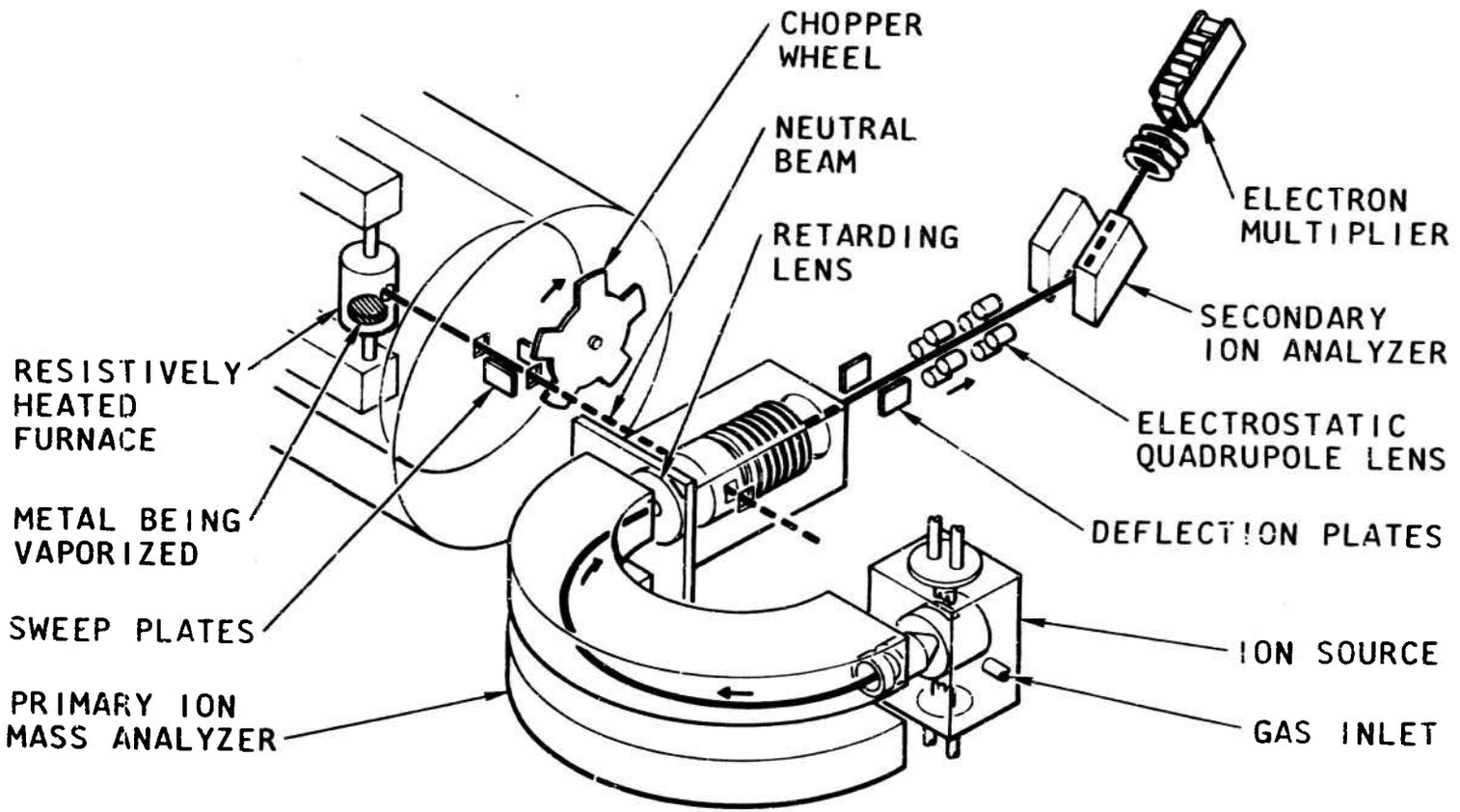

Fig. 1. Crossed ion and neutral beam apparatus

when making measurements. The cross sections have been corrected for the isotope effect created by collecting only those which have this mass. The output from the multiplier passes successively through a preamplifier, a 100-Hz narrow-band amplifier, and a phase-sensitive detector, and is then integrated. The output is presented on a chart recorder.

The primary ion beam intensity is measured at the interaction region with a Faraday cup which can be moved into the collision region when desired. The primary ion energy is determined from retarding potential measurements. All surfaces at the interaction region and the Faraday cup are coated with alkadag, and the interaction region is normally maintained at a temperature of 120°C to minimize surface-charging.

Because interest in the present work extends down to small collision energies, it was necessary to use only weak extraction fields at the collision region. As a result, the secondary ions were not collected with 100% efficiency. To obtain absolute cross sections for production of various secondary ions, it was necessary, therefore, to determine their overall detection efficiency. This latter consideration is governed by a number of factors, including the multiplier gain and the efficiency of transmission of the secondary ions from the interaction region to the multiplier.

The gain of the multiplier-amplifier-recorder system is measured by modulating the primary ions prior to their entering the collision region. The ion current signal is first measured with the movable Faraday cup and then, after traversing the secondary mass spectrometer multiplier-amplifier system, by the recorder. Transmission of the primary ion through the second mass spectrometer was observed to be 92%. Table 1 shows the system gain for several species of ions impinging upon the multiplier.

The major experimental uncertainty is associated with the collection efficiency for the secondary ions. The uncertainty arises because collection fields sufficiently large to ensure total collection of the secondary ions

Table 1

SYSTEM GAIN FOR SEVERAL INCIDENT IONS[a]

Ion Mass	Ion Species	System Gain
1	H^+	1.0×10^{13}
2	H_2^+	1.4×10^{13}
4	He^+	1.4×10^{13}
12	C^+	1.5×10^{13}
14	N^+	1.8×10^{13}
16	O^+	1.6×10^{13}
18	H_2O^+	1.7×10^{13}
23	Na^+	7.7×10^{12}
24	Mg^+	8.7×10^{12}
28	N_2^+	1.0×10^{13}
28	CO^+	1.1×10^{13}
30	NO^+	1.0×10^{13}
32	O_2^+	1.0×10^{13}
39	K^+	5.7×10^{12}
40	Ar^+	6.0×10^{12}
40	Ca^+	4.7×10^{12}
44	CO_2^+	8.7×10^{12}
56	Fe^+	3.1×10^{12}

[a]For an ion energy of 2365 V impinging on the multiplier

cannot be employed due to the influence these fields would exert on the motion of low-energy primary ions. While measurements of the variation of collection efficiency with the strength of the extraction field may readily be made at high primary ion energies, these results are not necessarily relevant to the low-energy regime, where the dynamics of the charge transfer process may be different. Interpretations of the present charge transfer data obtained using weak collection fields is, therefore, based on the assumption that at energies above a few eV, the secondary ions are produced by simple electron transfer in collisions involving little momentum transfer, and that as a result, the collection efficiency is independent of both the nature and the energy of the primary ions. It is implicit in this assumption that the energy defect in the reaction is small, since energy not expended in excitation of the products must appear as kinetic energy and, therefore, would influence the collection efficiency.

A number of charge transfer reactions for which absolute cross sections had been previously determined were tabulated. Using the same experimental conditions and the detection efficiencies deduced from measurements of the primary beam, as well as the same signal strengths and detector sensitivity, the collection efficiency of our instrument is obtained by comparing our measured cross sections with the best tabulated values. The efficiencies so obtained, and illustrated in Table 2, varied by 20%; this may represent a real variation in the collection efficiency or simply reflect the discrepancies in the published cross-section values. In the present work, a collection of between 70 and 80% is used in the evaluation of the cross sections from measurements of the neutral beam density, the primary ion beam intensity, the dimensions of the neutral beam at the interaction zone, the system gain, and the recorded signal.

Table 2

COLLECTION EFFICIENCY OF SECONDARY IONS PRODUCED BY CHARGE EXCHANGE AT INTERACTION REGION

Reactants	Cross Section[a] (10^{-16} cm^2)	Secondary Ion Collection Efficiencies[b] (%)
$N_2^+:N_2$	29.0	80
$O_2^+:O_2$	15.5	68
$N^+:O_2$	16.5	74

[a]The primary ions were produced by bombardment with 40-eV electrons. The ion energy used for these measurements was 400 eV.

[b]Assuming cross sections listed (taken as most representative of those reported in the literature).

2.2 NEUTRAL BEAM FORMATION AND MEASUREMENT

2.2.1 The Iron Beam

The neutral iron atom beam originates in a heated molecular effusion source (a Knudsen cell). This cell was constructed from a high-purity alumina crucible surrounded by a tungsten foil. Passage of current through the foil heated the crucible to a temperature at which the vapor pressure of the iron was sufficient to produce a usable beam of iron atoms. A pure iron wire placed inside the crucible was used as the source of iron vapor. The heat loss from the crucible-foil assembly was minimized by using small mounting tubes and surrounding the total furnace with two sets of heat shields. The neutral beam was formed by effusion of the iron vapor from a small hole in the side of the crucible. The temperature of the crucible was determined using an optical pyrometer. Care was taken when using this instrument to ensure

that the temperature obtained was that of the crucible and not that of the surrounding foil or heat shields. Using the measured temperature, the vapor pressure of the iron in the crucible was determined.

The cosine law of molecular effusion[11] was applied to determine the beam density, knowing the equilibrium vapor pressure of the iron in the Knudsen cell at a particular temperature. The number density, n, in the beam at the interaction region is then computed under effusive flow condition to be

$$n = \frac{N_0 a}{4\pi r^2} , \qquad (1)$$

where N_0 is the number density in the furnace, a is the area of the aperture in the furnace, and r the distance from the aperture to the interaction region.

Calculation of the beam density with Eq. 1 has been used for the preliminary analysis of the data. One difficulty associated with this method is that the temperature must be quite accurately known, since the pressure is a sensitive function of the temperature. A small temperature gradient between the location measured by the optical pyrometer and the inside of the chamber could result in a large error in the calculated beam density and, thus, the cross section. In addition to this, any temperature gradient in the volume of the furnace containing the metal vapor would result in a corresponding uncertainty in the furnace pressure and, thus, in the neutral beam density.

To ensure that our temperature measurements were accurate and that our oven behaved correctly, a complementary technique was employed. This method utilized neutron activation analysis to determine the number of atoms deposited into the collector by the neutral beam in a known time period. For the iron experiments, a collector consisting of a polyethylene

bag attached to the end of a polyethylene cylinder was used. This assembly was located so that all the beam passing through the collision region entered the collector. Commercially available "Baggies" were chosen as the type of polyethylene bags, since they were found to be both free of contamination and thin-walled. After a deposition time of 30 hours, the bag was removed and sent to the Rad Tech Neutron Activation Analysis Facility for measurement. This method gave results in close agreement with the density calculated from the molecular effusion considerations.

2.2.2 Beams of Atmospheric Gases

The neutral beams of N_2, NO, and O_2 were formed by effusion from a tungsten source. As for the iron beam, the density of the beam was determined from the known pressure of the gas in the source, the area of the aperture in the source, and the distance from this aperture to the interaction region.

The vibrational energy in the neutral beam could be changed by resistive heating of the tungsten source. Due to the increased velocity of the neutral particles under these conditions, corrections were made to the beam density.

2.3 EXTRAPOLATION PROCEDURE

In our apparatus, the lowest ion energies obtainable are 1 eV or greater. Considerable interest in the charge exchange processes exist in the energy range from thermal to several eV. To obtain cross sections and rate coefficients in this region, an extrapolation procedure developed previously in this laboratory[12] has been used. This extrapolation procedure combines the energy dependence of the Rapp and Francis[13] resonant charge-transfer theory with the Gioumousis and Stevenson[14] complex format model.

The general formula developed for the total charge-exchange cross section takes into account the probabilities for charge exchange to occur both when a complex is formed and when it is not, and also corrects for nonrectilinear orbit when complex formation does not occur. The method can be formulated as follows.

The total charge-exchange cross section σ will be given by

$$\sigma = f\sigma_2 \quad \text{when} \quad 2\sigma_1 \leq \sigma_2 \quad , \tag{2}$$

or by

$$\sigma = (f - \tfrac{1}{2})\sigma_2 + \sigma_1 \quad \text{when} \quad 2\sigma_1 > \sigma_2 \quad , \tag{3}$$

where f is the fraction of collisions resulting in complex formation which decays into the charge-exchange channel, and σ_2 is the Gioumousis and Stevenson complex formation model cross section,[14] represented by

$$\sigma_2 = \pi\left(\frac{2e^2\alpha}{E}\right)^{\frac{1}{2}} \tag{4}$$

in which e is the electronic charge, α is the polarizability of the neutral, and E is the barycentric interaction energy. Also, σ_1, which is given by

$$\sigma_1 = \sigma_0\left[1 + \left(\frac{\sigma_2}{4\sigma_0}\right)^2\right] \quad , \tag{5}$$

represents the Rapp and Francis resonant charge-exchange formula modified to take account of the curved orbits of the reactants. The form of the Rapp and Francis formula[13] is

$$\sigma^{\frac{1}{2}} = A - B \log E \quad , \tag{6}$$

where A and B are constants.

The extrapolation is carried out by fitting the modified Rapp and Francis formula (Eq. 5) to the high-energy portion of the measured data,

which is in the region where complex formation should be negligible. The calculated curve is then extended to lower energies using the test given with Eqs. 2 and 3 to evaluate when the measured data deviate from the form of Eq. 5. In this manner, the contribution of complex formation is determined and the calculated curve can be extended to energies below those measured. A computer program has been developed to perform the calculations.

The extrapolation technique was developed by assuming that the relative abundance of the various products emerging from the capture-formed complex is independent of the relative kinetic energy of the reactants; that is, f remains constant. If this condition is not met, the technique will not give valid rate coefficients at near-thermal energies. In general, whether or not the extrapolation technique is valid can be seen by observing whether the calculated cross-section curve fits the experimental data to the lowest energy of measurement. This comparison is made for all data given here.

3. REACTIONS OF IRON WITH ATMOSPHERIC IONS

Iron is known to be an important minor constituent of the upper atmosphere.[15,16] Its presence can probably be accounted for from the ablation of meteors. Even though this species is in low concentration, it can have an important effect on the chemistry of the upper atmosphere. Its low ionization potential (7.870 eV)[17] is such that it may undergo charge exchange with all common atmospheric ions. The iron ions, once formed, should have a long lifetime since radiative recombination is the only significant loss mechanism. Atomic ions such as iron can, therefore, retard the deionization of the disturbed atmosphere.

Reactions of iron with positive ions have been studied in the energy range from 1 to 500 eV. All but one of the processes studied involve charge transfer. For completeness, the processes that have been studied are listed below.

Charge-transfer reaction

1. $H^+ + Fe \rightarrow H + Fe^+$
2. $N^+ + Fe \rightarrow N + Fe^+$
3. $O^+ + Fe \rightarrow O + Fe^+$
4. $N_2^+ + Fe \rightarrow N_2 + Fe^+$
5. $NO^+ + Fe \rightarrow NO + Fe^+$
6. $O_2^+ + Fe \rightarrow O_2 + Fe^+$
7. $H_2O^+ + Fe \rightarrow H_2O + Fe^+$
8. $H_3O^+ + Fe \rightarrow H_2O + H + Fe^+$

Proton-transfer reaction

1. $H_3O^+ + Fe \rightarrow H_2O + FeH^+$

The absolute values of the charge-transfer and proton-transfer cross sections for the formation of ions or iron are presented and discussed below. The cross sections are shown as a function of incident ion energy in the energy range from approximately 2 to 500 eV.

The cross sections for the charge transfer of neutral iron with the ions H_2O^+, O_2^+, O^+, and H^+ are shown in Fig. 2, while those for charge transfer with N_2^+, NO^+, and N^+ are shown in Fig. 3. The charge transfer and proton transfer reactions involving H_3O^+ are shown in Fig. 4.

The cross-section curves shown in Figs. 2 and 3 are all very similar in that they show an increase in magnitude with decreasing ion energy. This increase is similar for all seven species shown. In addition to this, the absolute magnitudes of the cross-section curves are all quite large and show little variation from species to species. That is, at 10 eV all the cross sections fall between 10 and 35 x 10^{-16} cm^2, while at 500 eV the total range of cross sections is between 5 and 30 x 10^{-16} cm^2. It is interesting to note in this regard that H^+ and O^+ (see Fig. 2), which have similar ionization potentials, have cross-section curves that are essentially the same.

The explanation for the similarity in the magnitude of the cross sections for all species in Figs. 2 and 3 probably arises from the multiplicity of states which exist in the iron ion formed. Previous studies of charge transfer with metal atoms in this laboratory[5] have shown that only for cases of very near resonance are the cross sections large and show a decreasing behavior with increasing ion energy over the total energy range studied. In these cases, one can calculate that if the product ion or neutral or both are left in specific excited states, the energy defect for the reaction

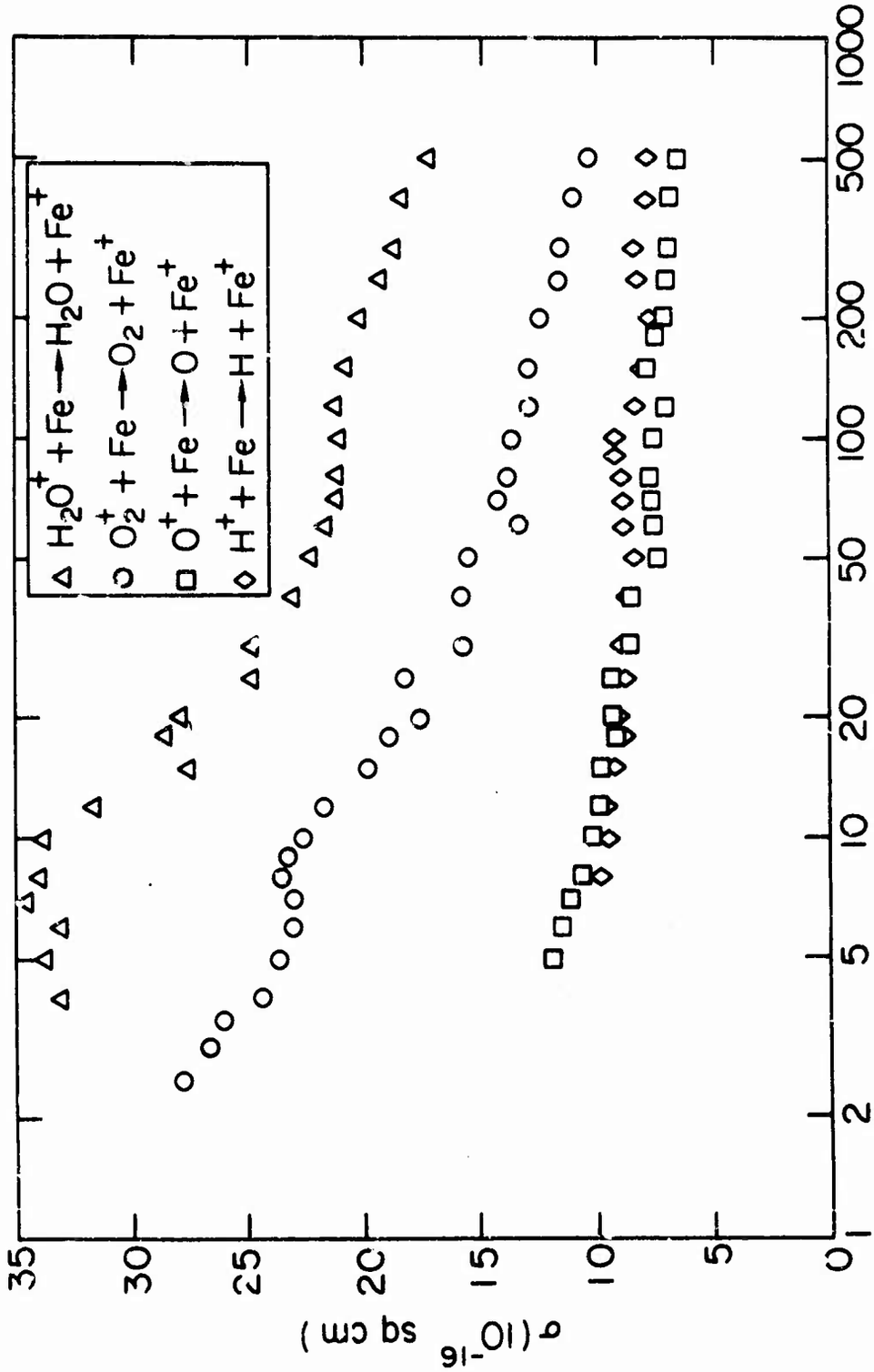

Fig. 2. Charge-transfer cross sections for H_2O^+, O_2^+, O^+, and H^+ ions impinging on neutral iron as a function of the energy of the incident ion

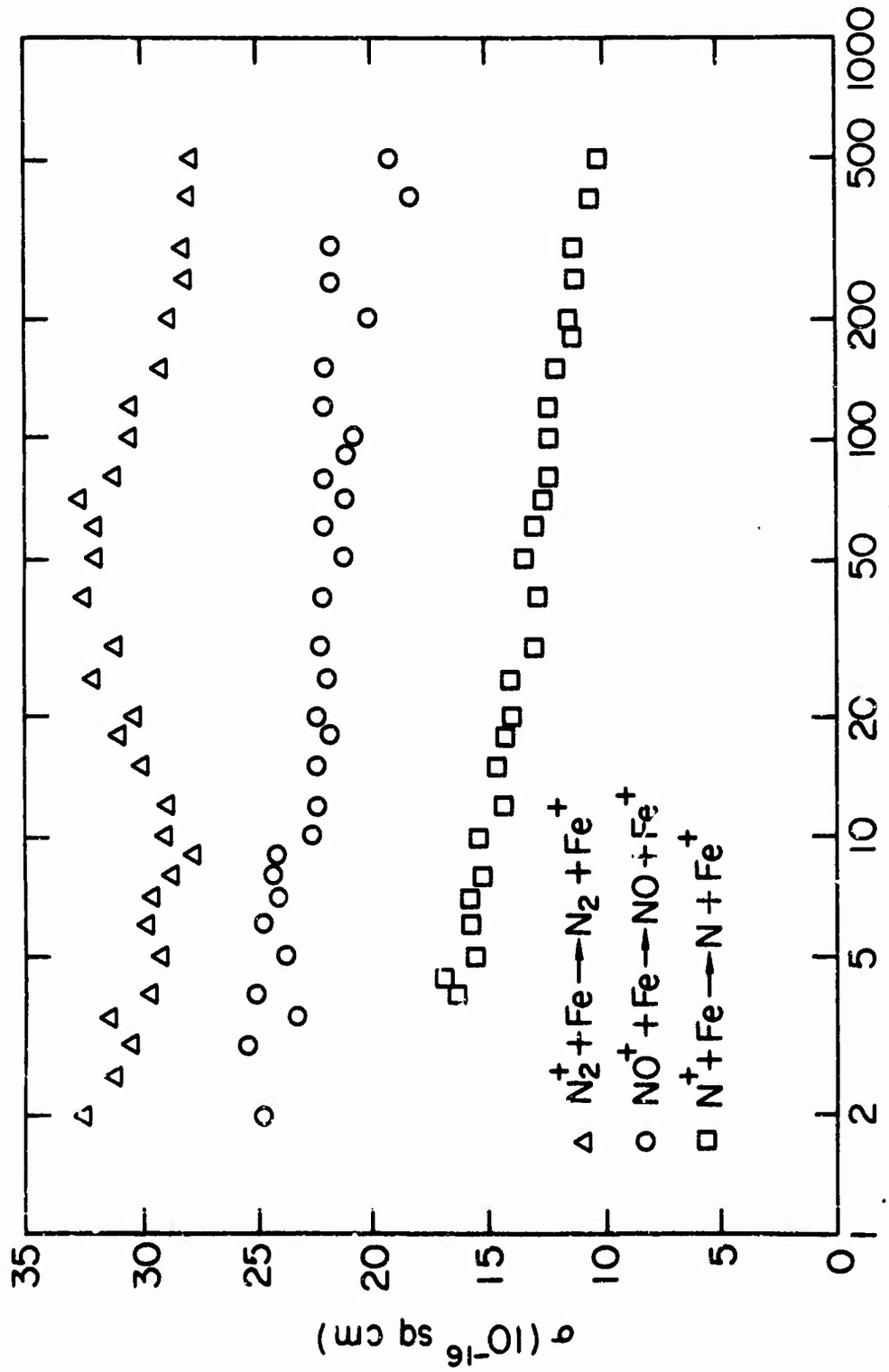

Fig. 3. Charge-transfer cross sections for N_2^+, NO^+, and N^+ ions impinging on neutral iron as a function of the energy of the incident ion

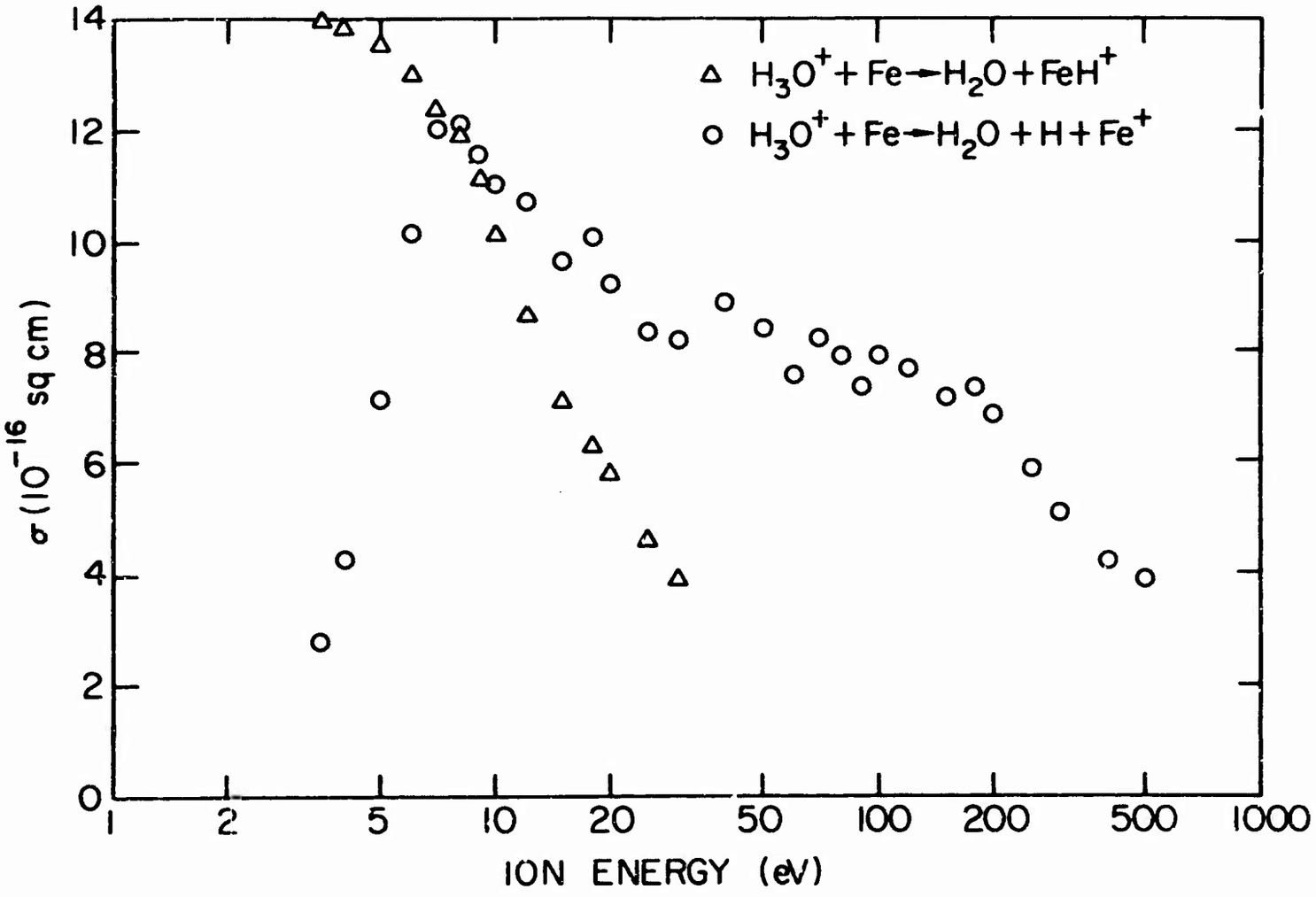

Fig. 4. Charge-transfer and prcton-transfer cross sections for H_3O^+ ions impinging on neutral iron as a function of the energy of the incident ion

will be small. In all cases involving metal atoms previously investigated, where the energy defect could be made small by formation of excited states, the cross sections were observed to be large while, for cases where no suitable states existed, the cross section was small. Iron, with its multitude of excited ion states, allows a near-resonance situation to exist for all cases shown in Figs. 2 and 3. As expected, the cross sections measured are all large.

The cross-section curves for the reaction of iron with H_3O^+ (see Fig. 4) differ from those discussed above. For the charge-transfer process leading to production of the neutral products H_2O and H, it can be seen from the diagram that the cross-section curve reaches a maximum at about 7 eV ion energy and then decreases at lower energies. Such behavior is indicative of a nonresonant process. The recombination energy of H_3O^+ is thought to be about 7 eV,[2] which is lower than the ionization potential of iron by about 0.87 eV. Since the process is endothermic, formation of an excited state cannot decrease this energy defect. The cross-section curve is, therefore, what would be expected in this case.

The proton-transfer cross section shown in Fig. 4 decreases rapidly with increasing ion energy. This behavior is what would be expected if an ion-molecule reaction involving complex formation was occurring.

The effects of long-lived excited states in the primary ion beam were investigated for all cases in which these species are known to exist (O^+, O_2^+, and NO^+). In all cases, very little change was observed in the cross-section curve when excited states were introduced. (A description of how the number of metastable species present in the primary ion beam is controlled is given in the following section.) The relative independence of the cross section on the state of excitation of the incident ion is not surprising, since the multitude of states available in the iron ion makes resonance possible for these species also. That is, the cross section for the ground-state ion is very similar to that for the excited-state.

Since the cross sections for charge exchange for H_2O^+, O_2^+, O^+, H^+, N_2^+, NO^+, and N^+ (Figs. 2 and 3) all have a high-energy behavior that follows the Rapp and Francis model[14] and a low-energy deviation from this model which can be interpreted by the Gioumousis and Stevenson model,[15] the extrapolation technique should provide a reasonable extension of the data. Tables 3 through 9 give the results of the extrapolation technique. The data given in the tables include the interaction energy in laboratory coordinates, center of mass coordinates, and temperature, as well as the cross-section and rate coefficient for the processes. Calculating the extrapolated cross-section for various values of the polarizability showed that the final values did not depend strongly on the polarizability. Both cross sections involving H_3O^+ were found to be unsuitable for extrapolation.

Table 3

CALCULATED CROSS SECTIONS AND RATE COEFFICIENTS FOR REACTION $H_2O^+ + Fe \rightarrow H_2O + Fe^+$

LAB ENERGY EV	CM ENERGY EV	CROSS SECTION SQ CM	RATE COEF (CU CM)/SEC	TEMP DEG K	VELOCITY CM/SEC
.0132	.0100	5.567942-14	2.095754-09	77.36	3.763965+04
.0512	.0388	2.043249-14	1.514496-09	300.00	7.412192+04
.1025	.0776	1.319677-14	1.383341-09	600.00	1.048242+05
.2050	.1551	9.070380-15	1.344628-09	1200.00	1.482438+05
.4100	.3102	6.648039-15	1.393751-09	2400.00	2.096485+05
.8199	.6205	5.172912-15	1.533.05-09	4800.00	2.964877+05
1.3214	1.0000	4.484806-15	1.688065-09	7736.05	3.763965+05
2.6429	2.0000	3.775320-15	2.009622-09	15472.09	5.323050+05
5.2857	4.0000	3.280574-15	2.469593-09	30944.18	7.527930+05
10.5714	8.0000	2.915196-15	3.103547-09	61888.37	1.064610+06
21.1429	16.0000	2.630140-15	3.959902-09	123776.74	1.505586+06
42.2857	32.0000	2.396657-15	5.103011-09	247553.47	2.129220+06
84.5714	64.0000	2.197535-15	6.617155-09	495106.95	3.011172+06
169.1429	128.0000	2.022236-15	8.611572-09	990213.90	4.258440+06
338.2857	256.0000	1.864173-15	1.122669-08	1980427.80	6.022344+06
676.5714	512.0000	1.719140-15	1.464171-08	3960855.59	8.516880+06
1321.4286	1000.0000	1.588864-15	1.891177-08	7736046.12	1.190270+07

Table 4

CALCULATED CROSS SECTIONS AND RATE COEFFICIENTS FOR REACTION $O_2^+ + Fe \rightarrow O_2 + Fe^+$

LAB ENERGY EV	CM ENERGY EV	CROSS SECTION SQ CM	RATE COEF (CU CM)/SEC	TEMP DEG K	VELOCITY CM/SEC
.0157	.0100	5.583815-14	1.718950-09	77.36	3.078451+04
.0609	.0388	1.885204-14	1.142857-09	300.00	6.062244+04
.1219	.0776	1.151624-14	9.873225-10	600.00	8.573308+04
.2438	.1551	7.464366-15	9.050162-10	1200.00	1.212449+05
.4875	.3102	5.177845-15	8.878253-10	2400.00	1.714662+05
.9750	.6205	3.846257-15	9.326773-10	4900.00	2.424898+05
1.5714	1.0000	3.249009-15	1.000192-09	7736.05	3.078452+05
3.1429	2.0000	2.653448-15	1.155202-09	15472.09	4.353584+05
6.2857	4.0000	2.250432-15	1.385569-09	30944.18	6.156903+05
12.5714	8.0000	1.957626-15	1.704012-09	61888.37	8.707176+05
25.1429	16.0000	1.727835-15	2.127684-09	123776.74	1.231381+06
50.2857	32.0000	1.538652-15	2.678407-09	247553.47	1.741435+06
100.5714	64.0000	1.373631-15	3.382526-09	495106.95	2.462761+06
201.1429	128.0000	1.226613-15	4.272331-09	990213.90	3.482870+06
402.2857	256.0000	1.093148-15	5.384331-09	1980427.80	4.925522+06
804.5714	512.0000	9.700694-16	6.757252-09	3960855.59	6.965741+06
1571.4286	1000.0000	8.598275-16	8.370350-09	7736046.12	9.734918+06

Table 5

CALCULATED CROSS SECTIONS AND RATE COEFFICIENTS FOR REACTION $O^+ + Fe \rightarrow O + Fe^+$

LAB ENERGY EV	CM ENERGY EV	CROSS SECTION SQ CM	RATE COEF (CU CM)/SEC	TEMP DEG K	VELOCITY CM/SEC
.0129	.0100	1.616922-13	6.367389-09	77.36	3.937968+04
.0499	.0388	4.455095-14	3.454859-09	300.00	7.754849+04
.0997	.0776	2.325706-14	2.550604-09	600.00	1.096701+05
.1994	.1551	1.231575-14	1.910185-09	1200.00	1.550970+05
.3989	.3102	6.695594-15	1.468611-09	2400.00	2.193402+05
.7977	.6205	3.808470-15	1.181364-09	4800.00	3.101939+05
1.2857	1.0000	2.685561-15	1.057565-09	7736.05	3.937968+05
2.5714	2.0000	1.744154-15	9.713416-10	15472.09	5.569128+05
5.1429	4.0000	1.255156-15	9.885527-10	30944.18	7.875937+05
10.2857	8.0000	9.967894-16	1.110250-09	61888.37	1.113826+06
20.5714	16.0000	8.555023-16	1.347576-09	123776.74	1.575187+06
41.1429	32.0000	7.733206-16	1.722689-09	247553.47	2.227651+06
82.2857	64.0000	7.207700-16	2.270696-09	495106.95	3.150375+06
164.5714	128.0000	6.829577-16	3.042783-09	990213.90	4.455303+06
329.1429	256.0000	6.524255-16	4.110770-09	1980427.80	6.300749+06
658.2857	512.0000	6.254886-16	5.573482-09	3960855.59	8.910605+06
1285.7143	1000.0000	6.012034-16	7.486756-09	7736046.12	1.245295+07

Table 6

CALCULATED CROSS SECTIONS AND RATE COEFFICIENTS FOR REACTION $H^+ + Fe \rightarrow H + Fe^+$

LAB ENERGY EV	CM ENERGY EV	CROSS SECTION SQ CM	RATE COEF (CU CM)/SEC	TEMP DEG K	VELOCITY CM/SEC
.0102	.0100	9.389124-14	1.385994-08	77.36	1.401533+05
.0395	.0388	2.661630-14	7.346022-09	300.00	2.759971+05
.0789	.0776	1.369960-14	5.346820-09	600.00	3.903188+05
.1579	.1551	7.191820-15	3.969843-09	1200.00	5.519942+05
.3158	.3102	3.948299-15	3.082183-09	2400.00	7.806376+05
.6316	.6205	2.352999-15	2.597683-09	4800.00	1.103988+06
1.0179	1.0000	1.763760-15	2.471969-09	7736.05	1.401533+06
2.0357	2.0000	1.299640-15	2.575974-09	15472.09	1.982067+06
4.0714	4.0000	1.079745-15	3.026598-09	30944.18	2.803086+06
8.1429	8.0000	9.737570-16	3.860104-09	61888.37	3.964135+06
16.2857	16.0000	9.178652-16	5.145674-09	123776.74	5.606133+06
32.5714	32.0000	9.817039-16	6.990386-09	247553.47	7.928269+06
65.1429	64.0000	8.514932-16	9.547112-09	495106.95	1.121227+07
130.2857	128.0000	8.214796-16	1.302582-08	990213.90	1.585654+07
260.5714	256.0000	7.897125-16	1.770893-09	1980427.80	2.242453+07
521.1429	512.0000	7.558902-16	2.397160-08	3960855.59	3.171308+07
1017.8571	1000.0000	7.216115-16	3.198209-08	7736046.12	4.432037+07

Table 7

CALCULATED CROSS SECTIONS AND RATE COEFFICIENTS FOR REACTION $N_2^+ + Fe \rightarrow N_2 + Fe^+$

LAB ENERGY EV	CM ENERGY EV	CROSS SECTION SQ CM	RATE COEF (CU CM)/SEC	TEMP DEG K	VELOCITY CM/SEC
.0150	.0100	2.029867-14	9.455910-10	77.36	3.215339+04
.0582	.0388	6.784971-15	4.236050-10	300.00	6.331807+04
.1163	.0776	4.654108-15	3.630260-10	600.00	8.954529+04
.2327	.1551	3.124446-15	3.330042-10	1200.00	1.266361+05
.4654	.3102	2.742412-15	4.511402-10	2400.00	1.790906+05
.9307	.6205	2.755137-15	6.978074-10	4800.00	2.532723+05
1.5000	1.0000	3.022121-15	9.074071-10	7736.05	3.215336+05
3.0000	2.0000	2.928153-15	1.331840-09	15472.09	4.547174+05
6.0000	4.0000	3.011714-15	1.938736-09	30944.18	6.430675+05
12.0000	8.0000	3.057304-15	2.780419-09	61888.37	9.094349+05
24.0000	16.0000	3.056022-15	3.944475-09	123776.74	1.286135+06
48.0000	32.0000	3.046327-15	5.540872-09	247553.47	1.818870+06
96.0000	64.0000	3.012291-15	7.722470-09	495106.95	2.572270+06
192.0000	128.0000	2.946502-15	1.069717-08	990213.90	3.637739+06
384.0000	256.0000	2.856534-15	1.474700-08	1980427.80	5.144540+06
768.0000	512.0000	2.793359-15	2.025381-08	3960855.59	7.275479+06
1500.0000	1000.0000	2.698605-15	2.743585-08	7736046.12	1.015779+07

Table 8

CALCULATED CROSS SECTIONS AND RATE COEFFICIENTS FOR REACTION $NO^+ + Fe \rightarrow NO + Fe^+$

LAB ENERGY EV	CM ENERGY EV	CROSS SECTION SQ CM	RATE COEF (CU CM)/SEC	TEMP DEG K	VELOCITY CM/SEC
.0154	.0100	5.103344-14	1.604176-09	77.36	3.143074+04
.0596	.0388	1.490425-14	9.163095-10	300.00	6.289501+04
.1191	.0775	8.492494-15	7.424953-10	600.00	8.753277+04
.2382	.1551	5.347132-15	6.619216-10	1200.00	1.237900+05
.4764	.3102	3.804333-15	6.660960-10	2400.00	1.750655+05
.9529	.6205	3.049601-15	7.550205-10	4800.00	2.475801+05
1.5357	1.0000	2.766522-15	8.695382-10	7736.05	3.143074+05
3.0714	2.0000	2.531694-15	1.125332-09	15472.09	4.444977+05
6.1429	4.0000	2.402054-15	1.509967-09	30944.18	6.286147+05
12.2857	8.0000	2.317925-15	2.060536-09	61888.37	8.889955+05
24.5714	16.0000	2.250380-15	2.829998-09	123776.74	1.257229+06
49.1429	32.0000	2.189037-15	3.893089-09	247553.47	1.777991+06
98.2857	64.0000	2.126955-15	5.348143-09	495106.95	2.514459+06
196.5714	128.0000	2.063121-15	7.336422-09	990213.90	3.555982+06
393.1429	256.0000	1.997389-15	1.004476-08	1980427.80	5.028973+06
785.2857	512.0000	1.930214-15	1.372761-08	3960855.59	7.111964+06
1535.7143	1000.0000	1.864472-15	1.853143-08	7736046.12	9.939272+06

Table 9

CALCULATED CROSS SECTIONS AND RATE COEFFICIENTS FOR REACTION $N^+ + Fe \rightarrow N + Fe^+$

LAB ENERGY EV	CM ENERGY EV	CROSS SECTION SQ CM	RATE COEF (CU CM)/SEC	TEMP DEG K	VELOCITY CM/SEC
.0125	.0100	6.258106-14	2.597729-09	77.36	4.150983+04
.0485	.0388	1.800935-14	1.472144-09	300.00	8.174328+04
.0969	.0776	9.920800-15	1.146869-09	600.00	1.156025+05
.1939	.1551	5.789255-15	9.464654-10	1200.00	1.634866+05
.3878	.3102	3.684593-15	8.518959-10	2400.00	2.312049+05
.7756	.6205	2.610338-15	9.535104-10	4800.00	3.269731+05
1.2500	1.0000	2.191034-15	9.094987-10	7736.05	4.150983+05
2.5000	2.0000	1.830271-15	1.074438-09	15472.09	5.870377+05
5.0000	4.0000	1.625706-15	1.349656-09	30944.18	8.301966+05
10.0000	8.0000	1.495225-15	1.755506-09	61888.37	1.174075+06
20.0000	16.0000	1.398446-15	2.321970-09	123776.74	1.660393+06
40.0000	32.0000	1.316097-15	3.090394-09	247553.47	2.348151+06
80.0000	64.0000	1.239428-15	4.115874-09	495106.95	3.320787+06
160.0000	128.0000	1.164816-15	5.470328-09	990213.90	4.696301+06
320.0000	256.0000	1.091053-15	7.246309-09	1980427.80	6.641573+06
640.0000	512.0000	1.017996-15	9.561633-09	3960855.59	9.392603+06
1250.0000	1000.0000	9.483666-16	1.244879-08	7736046.12	1.312656+07

4. REACTIONS BETWEEN COMMON ATMOSPHERIC IONS AND NEUTRALS

The major emphasis during the last contract period has been to investigate how an ion molecule process can be affected by the internal energy of the reactants. Both the change in the reaction cross section and in the state of the final products have been considered. Studies of this nature have direct application in problems associated with an understanding of the chemistry of the upper atmosphere, since many species in the upper atmosphere will be found in vibrationally or electronically excited states. This program answers a direct DNA need.

The processes which have been considered this year are:

$$N^+ + N_2 \rightarrow N + N_2^+$$
$$N_2^+ + O_2 \rightarrow N_2 + O_2^+$$
$$N_2^+ + NO \rightarrow N_2 + NO^+$$
$$O^+ + N_2 \rightarrow O + N_2^+$$
$$O^+ + N_2 \rightarrow NO^+ + N$$

For all these reactions, the states of the primary ion beam have been changed to see the influence on the cross sections and the products. The vibrational states of the neutral particles have also been varied by heating the gases. Again, attempts were made to see changes in the reaction cross sections and products. More violent means of excitation will be used in the future to obtain higher vibrational levels and electronic metastables of the neutral species.

In the following sections, a brief explanation of how the state of excitation of the ion beam is regulated will be given, followed by the results obtained for each reaction studied.

4.1 CONTROL OF THE STATE OF EXCITATION OF THE PRIMARY ION BEAMS

The primary ion beam is formed in an electron impact source (see Fig. 1), the electron energy of which can be carefully controlled. If the electron energy is such that the gas in the ion source can be ionized but is not high enough to leave any ions in metastable state, then the primary ion beam will consist entirely of ground-state particles. Increasing the electron energy will lead to introduction of metastable ions into the beam. The ratio of ground to metastable states is generally a function of the electron energy at energies up to several times the ionization potential of the gas. Above this value, the ratio usually becomes constant. The transit time of the primary ion system is such that excited species with lifetimes less than about 1 μsec will have decayed before reaching the ion-neutral collision region.

When studying the effects of metastable ions in the primary ion beam, the following procedure is generally employed. For a fixed ion energy (that is, a fixed ion-neutral interaction energy), the electron energy in the primary ion source is varied over a range from the ionization potential of the primary ions to several times this ionization potential. A relative cross section for formation of the product ion under consideration is measured as a function of this electron impact energy. (If metastable ions are observed, their population can be determined in an auxiliary experiment.)[18] Three types of behavior are found: First, the relative cross section as a function of electron energy may be unchanged over the electron energy range. This implies a similar reaction cross section for ground and metastable states. Second, if the relative cross section

increases above the onset of metastable formation, the cross section for the excited ions is larger than that for the ground state. Third, if the relative cross section decreases above the onset of metastable formation, then of course the excited state cross section is smaller than that for the ground state.

In order to obtain absolute cross sections for each of the components of the ion beam, it is necessary to know the ratio of ground to metastable in the beam. Techniques for obtaining this ratio have been developed previously in this laboratory.[18]

4.2 $N^+ + N_2 \rightarrow N + N_2^+$

The data obtained for the charge transfer cross section are given in Table 10. For convenience, these data are displayed graphically in Fig. 5. From the diagram, it can be seen that the cross section is small and decreases with decreasing energy in the region between 1.5 and 4 eV. This behavior is expected since the process is endothermic by approximately 1 eV. The rise in the cross section at about 4 eV probably results from the onset of a second channel for reaction. This channel could result in N_2^+ being formed in the excited $B^2\Sigma_u^+$ state since this process is approximately 4 eV endothermic and could, therefore, have a threshold in the region found for the onset of the second process. This explanation for the curve shape has been used previously by Murad and Maier.[19]

The data presented here are in agreement with those of Murad and Maier,[19] although the present cross section tends to have a somewhat higher absolute value. The peak value (at 10 eV in the center of mass) is reported as 1.7×10^{-16} cm^2 here, while the value in Ref. 19 is 1.0×10^{-16} cm^2 at the same interaction energy.

No effect on the Neutral N_2 reactant due to additional internal energy could be observed when the N_2 gas in the neutral beam was heated to supply

Table 10

MEASURED CROSS SECTIONS FOR REACTION $N^+ + N_2 \rightarrow N + N_2^+$
(CENTER OF MASS AND
LABORATORY COLLISION ENERGIES GIVEN)

CM ENERGY	CROSS SECTION	LAB ENERGY
1.00	9.856626-18	1.50
1.33	1.310120-17	2.00
1.67	1.359024-17	2.50
2.00	1.843387-17	3.00
2.33	1.491769-17	3.50
2.67	1.984738-17	4.00
2.87	2.412279-17	4.30
3.00	2.572015-17	4.50
3.33	3.410492-17	5.00
3.67	3.764088-17	5.50
4.00	5.194206-17	6.00
4.13	6.006644-17	6.20
4.33	6.653541-17	6.50
4.67	8.487650-17	7.00
4.80	8.902007-17	7.20
5.00	9.093911-17	7.50
5.33	1.012562-16	8.00
5.67	1.112175-16	8.50
6.00	1.287791-16	9.00
6.33	1.414608-16	9.50
6.67	1.451114-16	10.00
7.00	1.577832-16	10.50
7.33	1.616695-16	11.00
7.67	1.697530-16	11.50
8.00	1.653406-16	12.00
8.33	1.730909-16	12.50
8.67	1.705075-16	13.00
9.33	1.680000-16	14.00
10.00	1.654925-16	15.00
10.67	1.534567-16	16.00
11.33	1.368547-16	17.00
12.00	1.278806-16	18.00
12.67	1.189065-16	19.00
13.33	1.129036-16	20.00
14.00	1.076889-16	21.00
16.67	9.591045-17	25.00
20.00	9.377910-17	30.00
26.67	9.149181-17	40.00
33.33	9.120166-17	50.00
40.00	8.710707-17	60.00
46.67	8.003411-17	70.00
53.33	7.672836-17	80.00
66.67	7.764179-17	100.00
80.00	7.307463-17	120.00
100.00	7.142880-17	150.00
120.00	7.485693-17	180.00
133.33	7.937313-17	200.00
166.67	7.413368-17	250.00
200.00	8.245853-17	300.00
266.67	9.311400-17	400.00
333.33	9.750895-17	500.00

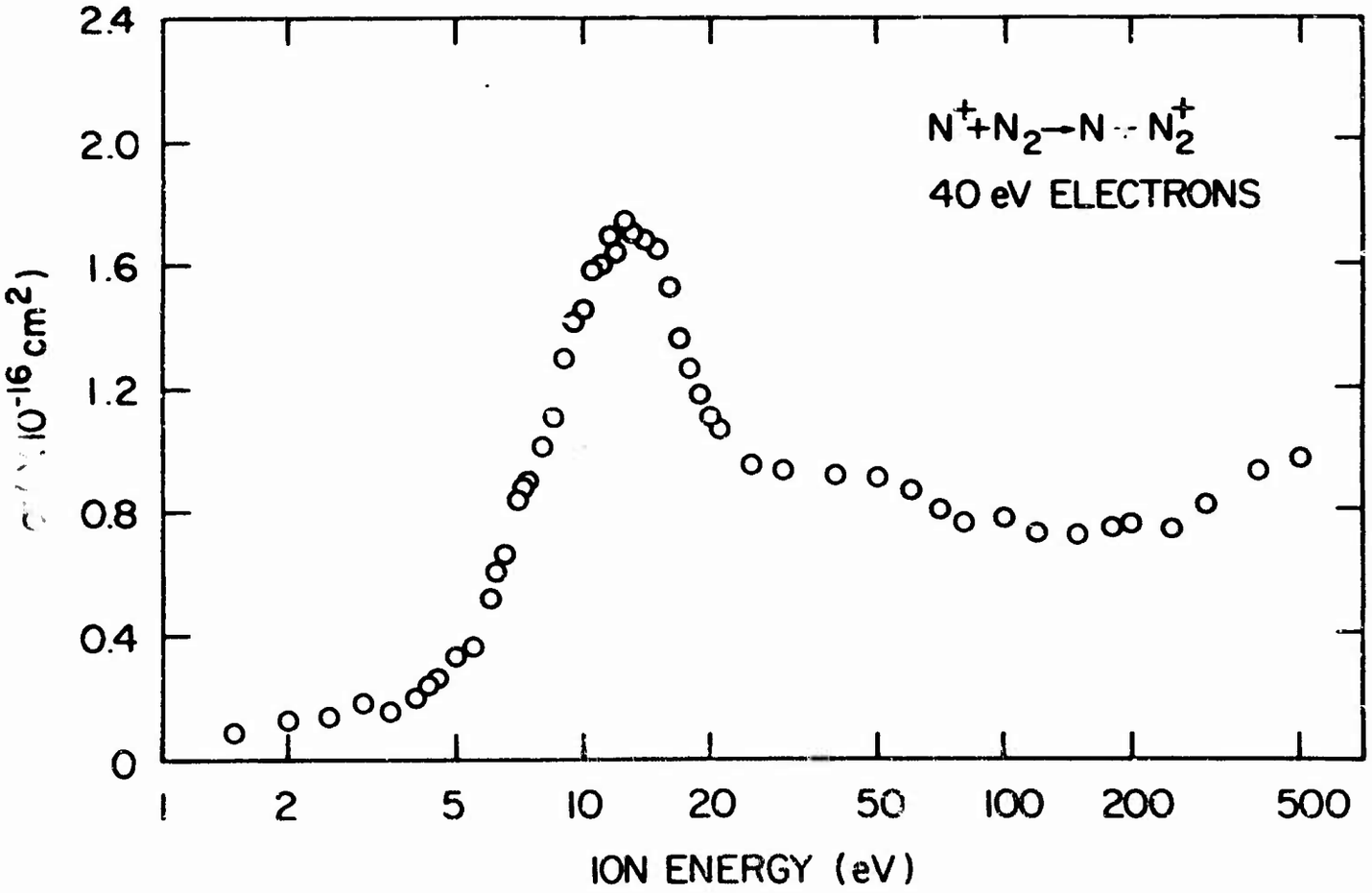

Fig. 5. Charge-transfer cross sections for N^+ ions incident on neutral nitrogen molecules as a function of the energy of the incident ion

the additional vibrational energy. This behavior is expected since no levels are close enough to cause resonance by vibrational excitation. Attempts were made to introduce the metastable $N^+(^1D)$ into the primary ion beam to observe the effect of this species on the cross section. Although a number of different gases containing N atoms were used to produce the N^+ beam, no evidence of the metastable could be found. Since several techniques were used without success to produce this species in the laboratory, one concludes that it is not easily formed. As a consequence, it is doubtful if $N^+(^1D)$ is a very common species in the upper atmosphere.

4.3 $N_2^+ + O_2 \rightarrow N_2 + O_2^+$

The charge transfer cross sections for N_2^+ on O_2 are shown in Fig. 6. Two different cases are represented: the case for very low electron energies (16.9 eV) in the primary ion source and the case for higher electron energies (40 eV). For convenience, the data for both electron energies are also presented in tabular form in Tables 11 and 12. Comparison of the two N_2^+ curves given in Fig. 6 reveals that the results obtained for high ion energies (above 50 eV) are similar in both cases. Below 50 eV, however, the cross section for N_2^+ ions with very little vibrational excitation (those ions formed by 16.9-eV electrons) is less than that for ions which can have appreciable vibrational energy. Franck-Condon calculations indicated that below the onset of the $N_2^+(A^2\Pi_u)$ state (~16.9 eV), all direct ionization of N_2 will produce ions in the zeroth and first vibrational levels of the ionic ground state.

The reason for the difference in the two curves shown in Fig. 6 probably lies in the fact that if sufficient energy is available internally in the N_2^+ ion, formation of the $O_2^+(a^4\Pi_u)$ state is possible. This process, which is nearly resonant, can be represented as

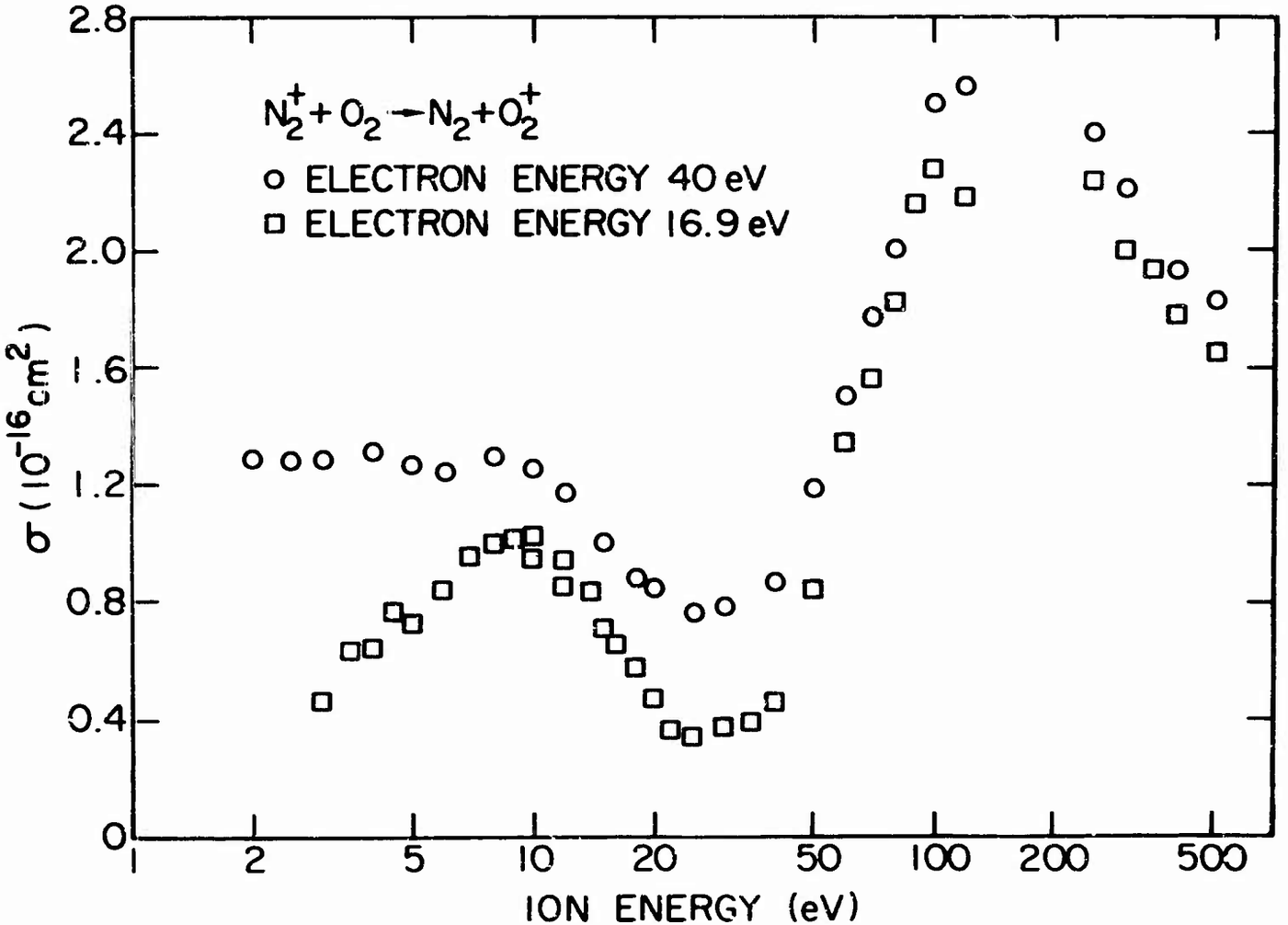

Fig. 6. Charge-transfer cross sections for N_2^+ ions incident on neutral oxygen molecules as a function of the energy of the incident ion. The cross sections for N_2^+ formed at two different primary ion-source electron energies are shown. The differences in the curves reflect the different vibration distributions present in the primary ion.

Table 11

MEASURED CRC SECTIONS FOR REACTION $N_2^+ + O_2 \rightarrow N_2 + O_2^+$
(CENTER OF MASS AND
LABORATORY COLLISION ENERGIES GIVEN)
(Source Electron Energy, 16.9 eV)

CM ENERGY	CROSS SECTION	LAB ENERGY
1.60	7.331971-17	3.00
1.87	8.899161-17	3.50
2.13	9.819614-17	4.00
2.40	1.216997-16	4.50
2.67	1.143787-16	5.00
3.20	1.319755-16	6.00
3.73	1.534599-16	7.00
4.27	1.576374-16	8.00
4.80	1.649693-16	9.00
5.33	1.533314-16	10.00
6.40	1.415544-16	12.00
7.47	1.319961-16	14.00
8.00	1.126797-16	15.00
8.53	1.035854-16	16.00
9.60	8.197460-17	18.00
10.67	7.419418-17	20.00
11.73	5.957362-17	22.00
13.33	5.524689-17	25.00
16.00	6.000699-17	30.00
18.67	6.223521-17	35.00
21.33	7.327466-17	40.00
26.67	1.323355-16	50.00
32.00	2.135124-16	60.00
37.33	2.468199-16	70.00
42.67	2.975438-16	80.00
48.00	3.425431-16	90.00
53.33	3.504567-16	100.00
64.00	3.453155-16	120.00
133.33	3.523832-16	250.00
160.00	3.216409-16	300.00
186.67	3.059421-16	350.00
213.33	2.900000-16	400.00
266.67	2.569073-16	500.00

Table 12

MEASURED CROSS SECTIONS FOR REACTION $N_2^+ + O_2 \rightarrow N_2 + O_2^+$
(CENTER OF MASS AND
LABORATORY COLLISION ENERGIES GIVEN)
(Source Electron Energy, 40 eV)

CM ENERGY	CROSS SECTION	LAB ENERGY
1.07	1.471869-16	2.00
1.33	1.716614-16	2.50
1.60	1.742053-16	3.00
1.87	1.755628-16	3.50
2.13	1.730457-16	4.00
2.67	1.861124-16	5.00
3.20	1.925134-16	6.00
3.73	2.011656-16	7.00
4.27	2.011656-16	8.00
5.33	1.916384-16	10.00
6.40	1.914435-16	12.00
8.00	1.586659-16	15.00
9.60	1.378357-16	19.00
10.67	1.341104-16	20.00
13.33	1.215376-16	25.00
16.00	1.234667-16	30.00
21.33	1.362392-16	40.00
26.67	1.882013-16	50.00
32.00	2.338336-16	60.00
37.33	2.746840-16	70.00
42.67	3.230842-16	80.00
53.33	3.855675-16	100.00
64.00	3.973642-16	120.00
80.00	5.337706-16	150.00
133.33	3.719693-16	250.00
160.00	3.433626-16	300.00
213.33	3.000000-16	400.00
266.67	2.822981-16	500.00

$$N_2^+(v=2 \text{ or } 3) + O_2(v=0) \rightarrow N_2(v=0) + O_2^+(a^4\Pi_u) \ .$$

The importance of the vibrational excitation of the N_2^+ in the charge transfer is further demonstrated by examining the primary ion-source electron-energy dependence of the cross section for 10-eV N_2^+ ions on O_2. This dependence, which is shown in Fig. 7, indicates that the cross section for the process changes rapidly for electron energies between 16 and 19 eV. At these energies, higher vibrational levels of the ground ionic state are probably being filled.

Experiments were also performed to see the effect of adding vibrational energy to the neutral O_2 species. For these experiments, the O_2 gas was heated in an iridium furnace. Here, a large change in the cross section for charge exchange was found, the cross section for the heated gas being larger than that for the cold gas. The reason for the change is probably the same here as for adding vibrational energy to the N_2^+ ions. The heated O_2 gas has some particles in high enough vibrational levels that the reaction becomes near-resonant for formation of the O_2^+ in the excited $(a^4\Pi_u)$ state. Work is continuing on this reaction.

4.4 $N_2^+ + NO \rightleftarrows N_2 + NO^+$

The results for the charge transfer between N_2^+ and NO are shown in Fig. 8. Numerical data are given in Table 13. The figure shows that the cross section for the reaction is invariant over the energy range from 10 to 500 eV. Below this range, the cross section increases rapidly down to the lowest energies measured. This increasing behavior is indicative of a near-resonant process. One possible mechanism which leads to a resonant condition is

$$N_2^+(X^2\Sigma_g^+) + NO(X^2\Pi) \rightarrow N_2(X^1\Sigma_g^+) + NO^+(a^3\Sigma^+) \ .$$

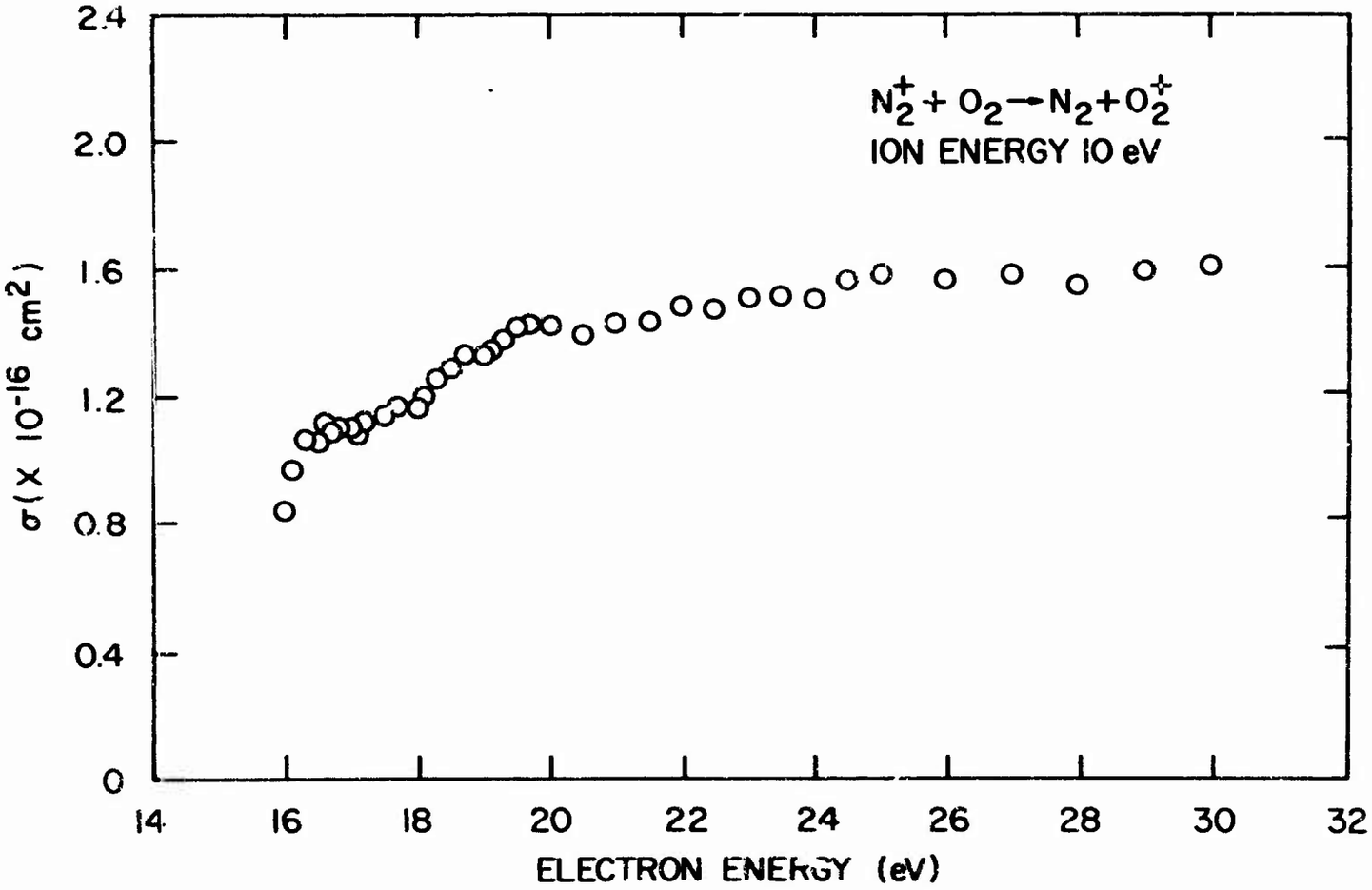

Fig. 7. Dependence of the charge-transfer cross section upon the ion-source electron energy for the reaction $N_2^+ + O_2 \rightarrow N_2 + O_2^+$. The N_2^+ had a kinetic energy of 10 eV.

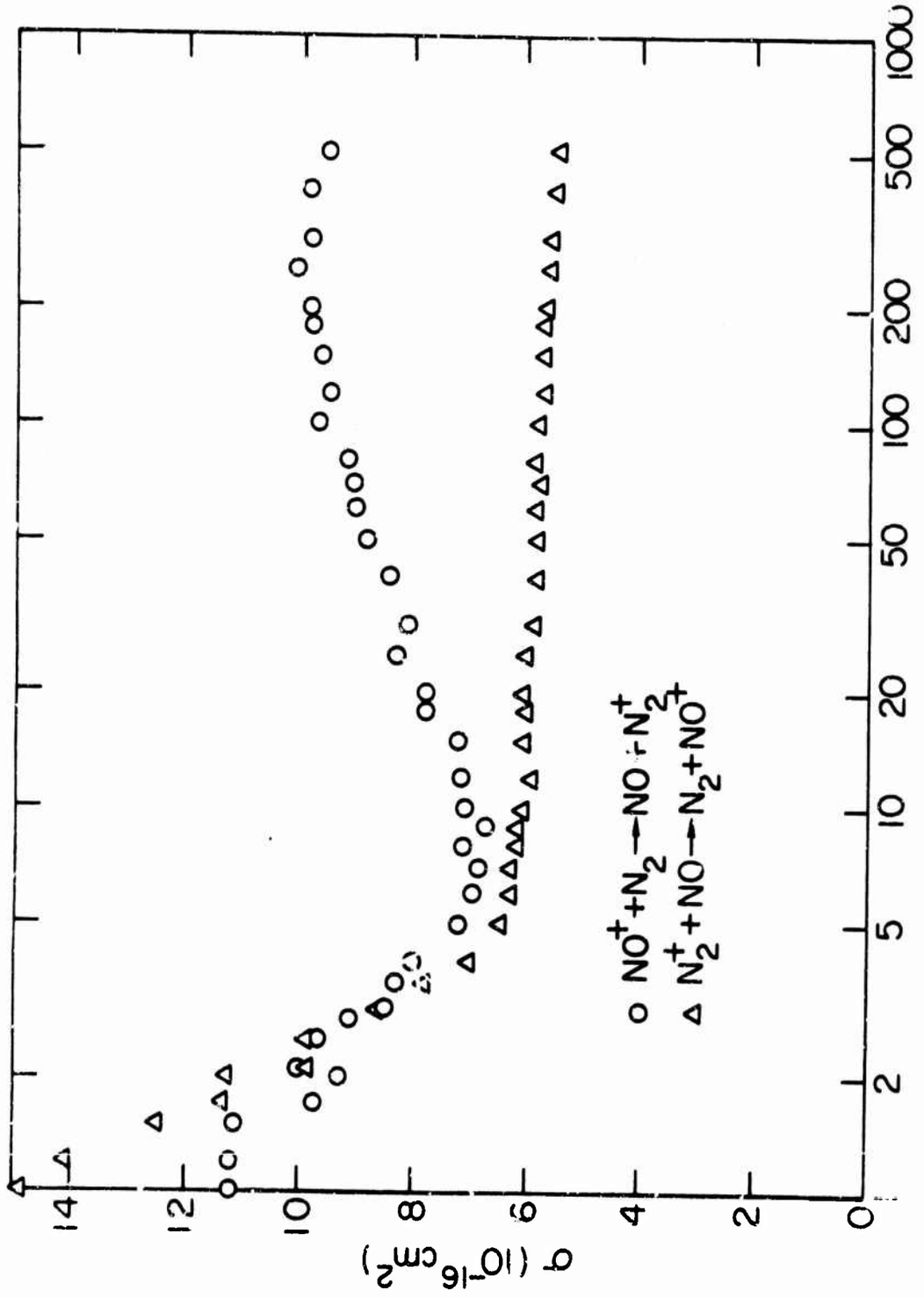

Fig. 8. Charge-transfer cross sections for N_2^+ ions impinging on neutral nitric oxide as a function of the energy of the incident ion and for the reverse reactions of NO^+ ions impinging on neutral nitrogen molecules. Note the reverse reactions are for NO^+ in the metastable $a^3\Sigma^+$ state.

Table 13

MEASURED CROSS SECTIONS FOR REACTION $N_2^+ + NO \rightarrow N_2 + NO^+$
(CENTER OF MASS AND
LABORATORY COLLISION ENERGIES GIVEN)

CM ENERGY	CROSS SECTION	LAB ENERGY
.36	1.690741-15	.70
.52	1.491064-15	1.00
.62	1.411647-15	1.20
.78	1.254490-15	1.50
.88	1.159505-15	1.70
1.03	1.140682-15	2.00
1.09	3.845950-16	2.10
1.29	9.968075-16	2.50
1.55	8.600549-16	3.00
2.07	7.039626-16	4.00
2.59	6.452587-16	5.00
3.10	6.355954-16	6.00
3.62	6.235358-16	7.00
4.14	6.156761-16	8.00
4.66	6.161167-16	9.00
5.17	6.038950-16	10.00
6.21	5.957529-16	12.00
7.76	6.029610-16	15.00
9.31	6.000000-16	19.00
10.34	6.024256-16	20.00
12.93	6.006857-16	25.00
15.52	5.915844-16	30.00
20.69	5.940000-16	40.00
25.86	5.840000-16	50.00
31.03	5.967342-16	60.00
36.21	5.697063-16	70.00
41.38	5.781010-16	80.00
51.72	5.791735-16	100.00
62.07	5.675901-16	120.00
77.59	5.688312-16	150.00
93.10	5.733818-16	180.00
103.45	5.631613-16	200.00
129.31	5.598678-16	250.00
155.17	5.585454-16	300.00
206.90	5.574545-16	400.00
258.62	5.418934-16	500.00

Huber[20] has shown that the $a^3\Sigma^+$ state of NO^+ lies at 15.6 eV above the neutral ground state. This energy is essentially the same as the ionization potential of N_2.

Figure 9 illustrates the primary ion-source electron-energy dependence for the reaction of N_2^+ on NO. This energy dependence is for 5-eV N_2^+ ions on NO. The figure shows little dependence of the cross section on the state of excitation of the N_2^+ ion. Since N_2^+ has no low-lying metastable electronic states, the small effect observed must be due to vibrational excitation of the N_2^+. One explanation as to why there should be any effect at all in what appears to be a near-resonant process may be due to the Franck-Condon factors for the process. That is, formation of the NO^+ ($a^3\Sigma^+$) state in a slightly higher vibrational level may be more probable than formation of the zeroth vibrational level. This process should require the N_2^+ to have some vibrational excitation, and a slight electron-energy dependence may, therefore, be expected.

If the mechanism for the N_2^+, NO charge transfer is that suggested above, one would predict that the reverse reaction would not occur for NO^+ in the ground ionic state but that there should be a large cross section for NO^+ in the metastable $a^3\Sigma^+$ state. Figure 10 gives the primary ion-source electron-energy dependence for this reverse process. The data are for 10-eV NO^+ ions in collision with N_2. The results shown in this diagram are what would be expected. Below 16 eV, the cross section for charge transfer is very small but increases rapidly at higher electron energies as a larger fraction of the beam becomes excited. The fulfillment of the prediction about the electron-energy dependence for the reaction of NO^+ with N_2 indicates that the proposed mechanism for the reaction is correct.

The charge transfer cross section for $NO^+(a^3\Sigma^+)$ on N_2 is presented in Fig. 8. Numerical data are given in Table 14.

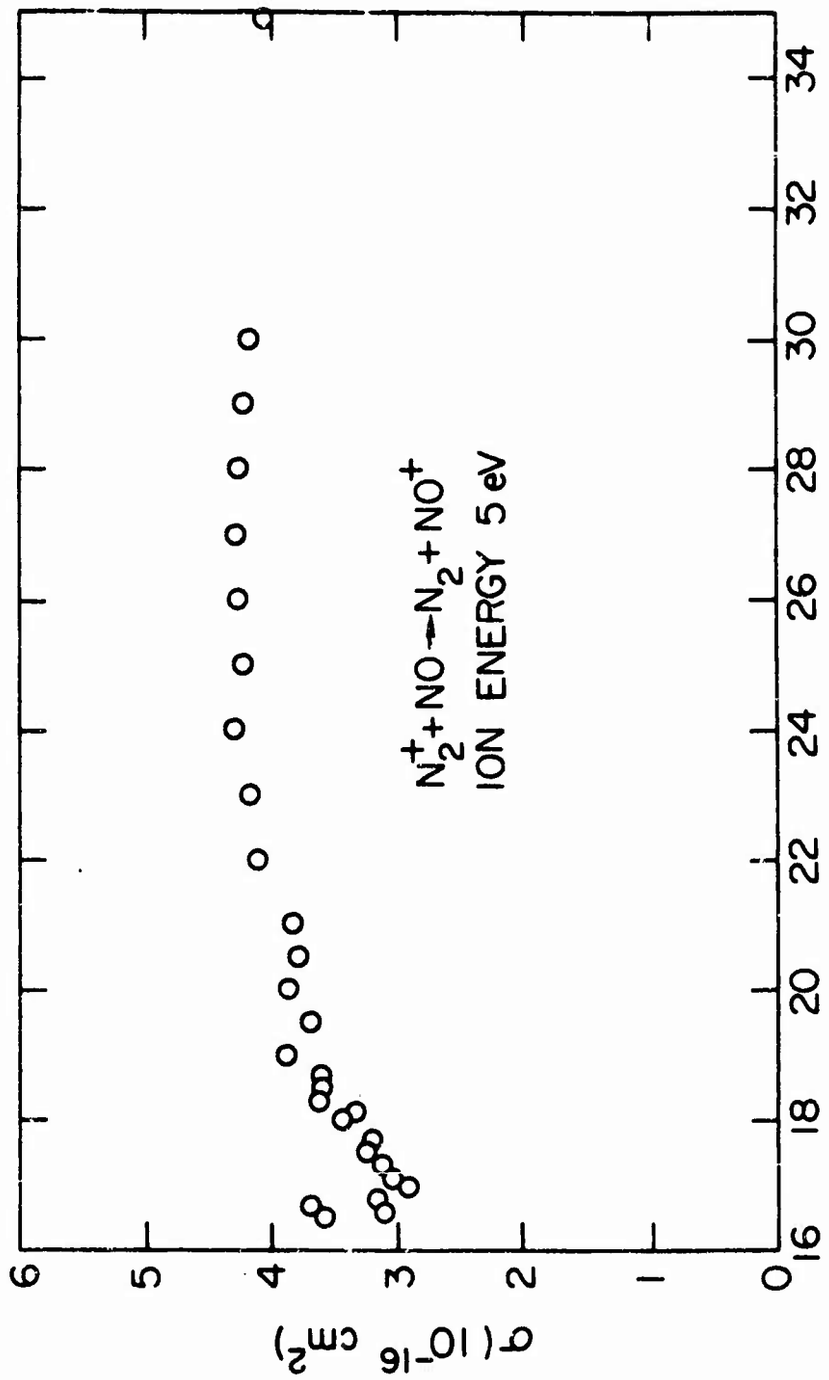

Fig. 9. Dependence of the charge-transfer cross section upon the ion source electron energy for the reaction $N_2^+ + NO \rightarrow N_2 + NO^+$. The N_2^+ had a kinetic energy of 5 eV.

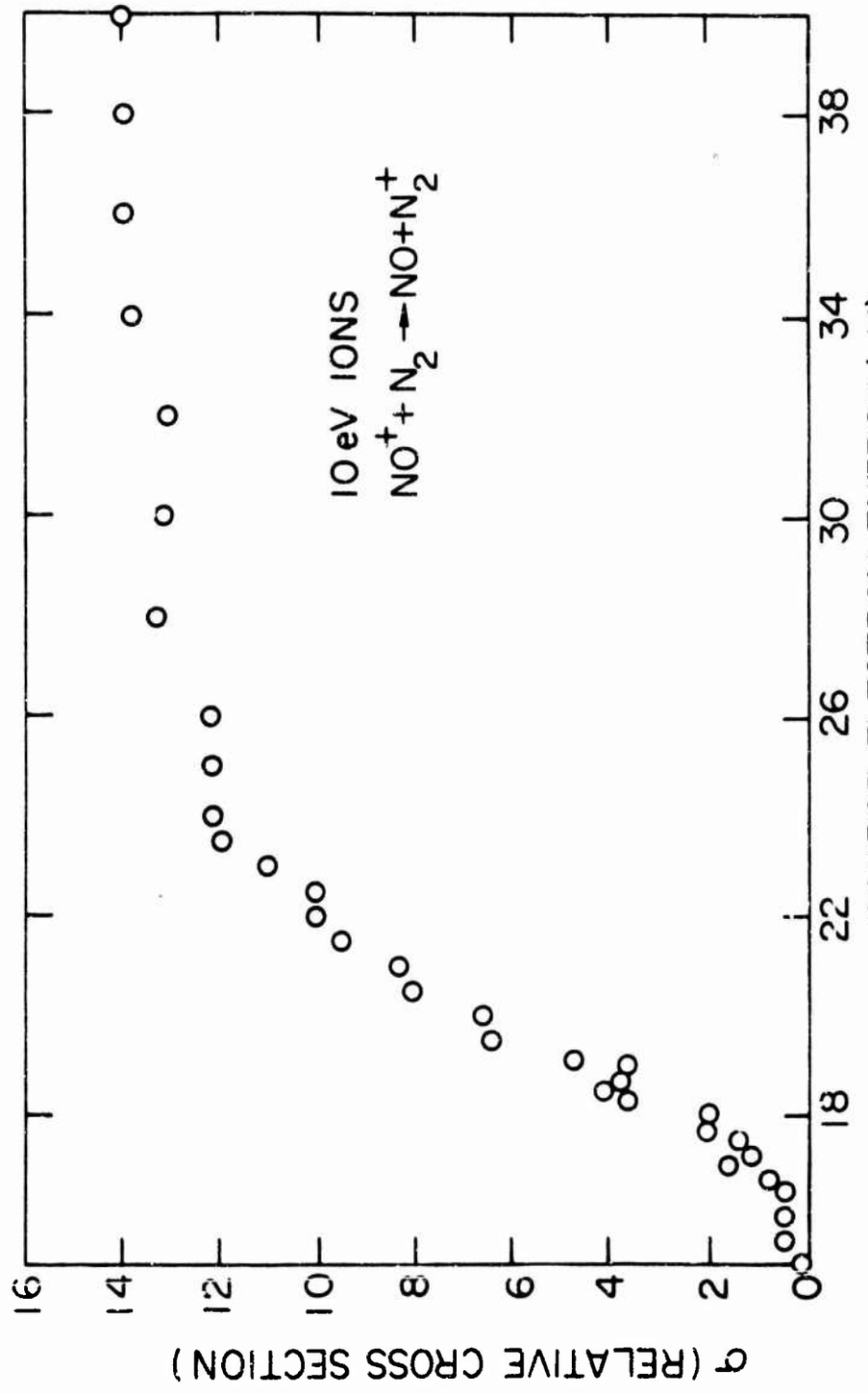

Fig. 10. Dependence of the charge-transfer cross section upon the ion-source electron energy for the reaction $NO^+ + N_2 \rightarrow NO + NO^+$. The NO^+ had a kinetic energy of 10 eV.

Table 14

MEASURED CROSS SECTION FOR REACTION $NO^+ + N_2 \rightarrow NO + N_2^+$
(CENTER OF MASS AND
LABORATORY COLLISION ENERGIES GIVEN)

CM ENERGY	CROSS SECTION	LAB ENERGY
.48	1.141591-15	1.00
.58	1.191225-15	1.20
.72	1.132541-15	1.50
.82	9.789002-16	1.70
.97	9.313842-16	2.00
1.01	1.000096-15	2.10
1.21	9.776468-16	2.50
1.35	9.171569-16	2.80
1.45	8.542839-16	3.00
1.69	8.306864-16	3.50
1.93	7.799191-16	4.00
2.17	5.837847-16	4.50
2.41	6.438588-16	5.00
2.90	6.501487-16	6.00
3.38	6.647042-16	7.00
3.86	6.911412-16	8.00
4.34	6.870266-16	9.00
4.83	7.201930-16	10.00
5.79	7.196084-16	12.00
7.24	7.264686-16	15.00
8.69	7.783796-16	18.00
9.66	7.958197-16	20.00
12.07	8.270283-16	25.00
14.48	8.127692-16	30.00
19.31	8.405861-16	40.00
24.14	8.771512-16	50.00
28.97	8.959473-16	60.00
33.79	9.012488-16	70.00
38.62	9.177997-16	80.00
48.28	9.705248-16	100.00
57.93	9.451752-16	120.00
72.41	9.623602-16	150.00
86.90	9.786502-16	180.00
96.55	9.945575-16	200.00
120.69	1.036871-15	250.00
144.83	9.814069-16	300.00
193.10	9.850000-16	400.00
241.38	9.451752-16	500.00

The cross sections for charge transfer for both processes have been extrapolated to thermal energies. The values obtained in the extrapolation are given in Table 15 for the $N_2^+ + NO$ reaction and in Table 16 for the reverse process. The value obtained for the rate coefficient for the reaction $N_2^+ + NO$ at 300°K (8.1×10^{-10} cm^3/sec) agrees well with the value (5.0×10^{-10} cm^3/sec) obtained using other techniques.[21]

4.5 $O^+ + N_2 \rightarrow O + N_2^+$ and $O^+ + N_2 \rightarrow NO^+ + N$

The results obtained for these two reactions have been discussed in a paper which is being prepared for publication. A copy of the paper is included as an Appendix to this report. The remainder of this section will outline the results obtained for these reactions, and will discuss one aspect which was not included in the publication.

The principal result of the investigation of these two reactions is that O^+ in the ground state reacts with N_2 to form NO^+ with little N_2^+ being formed, while the metastable O^+ reacts to form N_2^+ (charge transfer) with virtually no NO^+ being formed. This reactions can be represented as

$$O^+(^4S^o) + N_2(X^2\Sigma_g^+) \rightarrow NO^+(X^1\Sigma^+) + N(^4S^o)$$

and

$$O^+(^2D) + N_2(X^2\Sigma_g^+) \rightarrow O(^3P) + N_2^+(A^2\Pi_u) .$$

This last reaction is resonant for formation of the $N_2^+(A^2\Pi_u)$ state in the first vibrational level.

The ion-molecule reaction leading to formation of NO^+ is exothermic for all reactants and products being in the ground state. The overall energies can be represented by:

Energy Available		Energy Required	
O^+(IP)	13.6 eV	N_2 bond	9.7 eV
NO bond	6.5 eV	NO^+(IP)	9.3 eV
	20.1 eV		19.0 eV

Table 15

CALCULATED CROSS SECTIONS AND RATE COEFFICIENTS FOR REACTION $N_2^+ + NO \rightarrow N_2 + NO^+$
(CENTER OF MASS AND LABORATORY COLLISION ENERGIES GIVEN)

LAB ENERGY EV	CM ENERGY EV	CROSS SECTION SQ CM	RATE COEF (CU CM)/SEC	TEMP DEG K	VELOCITY CM/SEC
.0193	.0100	4.159023-14	1.518188-09	77.36	3.650349+04
.0750	.0388	1.132560-14	8.141358-10	300.00	7.188453+04
.1499	.0776	5.980312-15	6.079589-10	600.00	1.016601+05
.2999	.1551	3.288503-15	4.727850-10	1200.00	1.437691+05
.5998	.3102	1.936555-15	3.937406-10	2400.00	2.033202+05
1.1996	.6205	1.259363-15	3.621147-10	4800.00	2.875381+05
1.9333	1.0000	1.002305-15	3.658764-10	7736.05	3.650349+05
3.8667	2.0000	7.919424-16	4.088302-10	15472.09	5.162372+05
7.7333	4.0000	6.857729-16	5.006620-10	30944.18	7.300697+05
15.4667	8.0000	6.308044-16	6.512894-10	61888.37	1.032474+06
30.9333	16.0000	6.006229-16	8.769931-10	123776.74	1.460139+06
61.8667	32.0000	5.821747-16	1.202161-09	247553.47	2.064949+06
123.7333	64.0000	5.690900-16	1.661901-09	495106.95	2.920279+06
247.4667	128.0000	5.583196-16	2.305803-09	990213.90	4.129898+06
494.9333	256.0000	5.484492-16	3.203243-09	1980427.80	5.840558+06
989.8667	512.0000	5.388515-16	4.450804-09	3960855.59	8.259796+06
1933.3333	1000.0000	5.296083-16	6.113499-09	7736046.12	1.154342+07

Table 16

MEASURED CROSS SECTIONS FOR REACTION $NO^+ + N_2 \rightarrow NO + N_2^+$
(CENTER OF MASS AND LABORATORY COLLISION ENERGIES GIVEN)

LAB ENERGY EV	CM ENERGY EV	CROSS SECTION SQ CM	RATE COEF (CU CM)/SEC	TEMP DEG K	VELOCITY CM/SEC
.0207	.0100	4.479258-14	1.635085-09	77.36	3.650349+04
.0803	.0388	1.059577-14	7.616722-10	300.00	7.188453+04
.1607	.0776	5.186131-15	5.272225-10	600.00	1.016601+05
.3213	.1551	2.677416-15	3.849296-10	1200.00	1.437691+05
.6426	.3102	1.543447-15	3.138139-10	2400.00	2.033202+05
1.2853	.6205	1.054894-15	3.033221-10	4800.00	2.875381+05
2.0714	1.0000	9.042737-16	3.300914-10	7736.05	3.650349+05
4.1429	2.0000	8.192163-16	4.223937-10	15472.09	5.162372+05
8.2857	4.0000	8.085152-16	5.902725-10	30944.18	7.300697+05
16.5714	8.0000	8.305037-16	8.574738-10	61888.37	1.032474+06
33.1429	16.0000	8.641575-16	1.261790-09	123776.74	1.460139+06
66.2857	32.0000	9.009126-16	1.860339-09	247553.47	2.064949+06
132.5714	64.0000	9.374225-16	2.737535-09	495106.95	2.920279+06
265.1429	128.0000	9.726334-16	4.016877-09	990213.90	4.129998+06
530.2857	256.0000	1.006437-15	5.878151-09	1980427.80	5.840558+06
1060.5714	512.0000	1.039064-15	8.582454-09	3960855.59	8.259796+06
2071.4286	1000.0000	1.069752-15	1.234859-08	7736046.12	1.154342+07

Therefore, the excess energy is 1.1 eV.

Figure 11 is a graphical representation of the cross section for this ion-molecule reaction. The figure shows that the cross section is small for very low interaction energies but increases at higher energies, peaking at about 14-eV ion energy. This behavior may indicate that an activation energy is needed.

One possible explanation for the apparent endothermicity of the reaction is that an intermediate molecule in the excited state $(\pi+\pi+\pi,\pi)$ state[22] is formed. The kinetics here are

$$O^+(^4S^o) + N_2(^1\Sigma_g^+) \rightarrow N_2O^+(\pi+\pi+\pi,\pi) \rightarrow NO^+(X^1\Sigma^+) + N(^4S^o) .$$

Formation of $N_2O^+(\pi+\pi+\pi,\pi)$:

Energy Available		Energy Required	
O^+(IP)	13.6 eV	$N_2O^+(\pi+\pi+\pi,\pi)$(IP)	16.4 eV
N_2-O bond	1.6 eV		
	15.2 eV		16.4 eV

The process leading to formation of N_2O^+ excited ion is, therefore, 1.2 eV endothermic.

Decay of N_2O^+ $(\pi+\pi+\pi,\pi)$

Energy Available		Energy Required	
$N_2O(\pi+\pi+\pi,\pi)$(IP)	16.4 eV	NO^+(IP)	9.3 eV
		NO-N bond	4.8 eV
	16.4 eV		14.1 eV

This process is, therefore, 2.3 eV exothermic.

Since the first process is 1.2 eV endothermic and the second 2.3 eV exothermic, the overall reaction has again an excess energy of 1.1 eV. Such a reaction scheme accounts for the apparent endothermicity of the reaction. This reaction has been discussed previously by Kauffman and Koski,[23] Giese,[24] and Schmeltekopf et al.[25, 26]

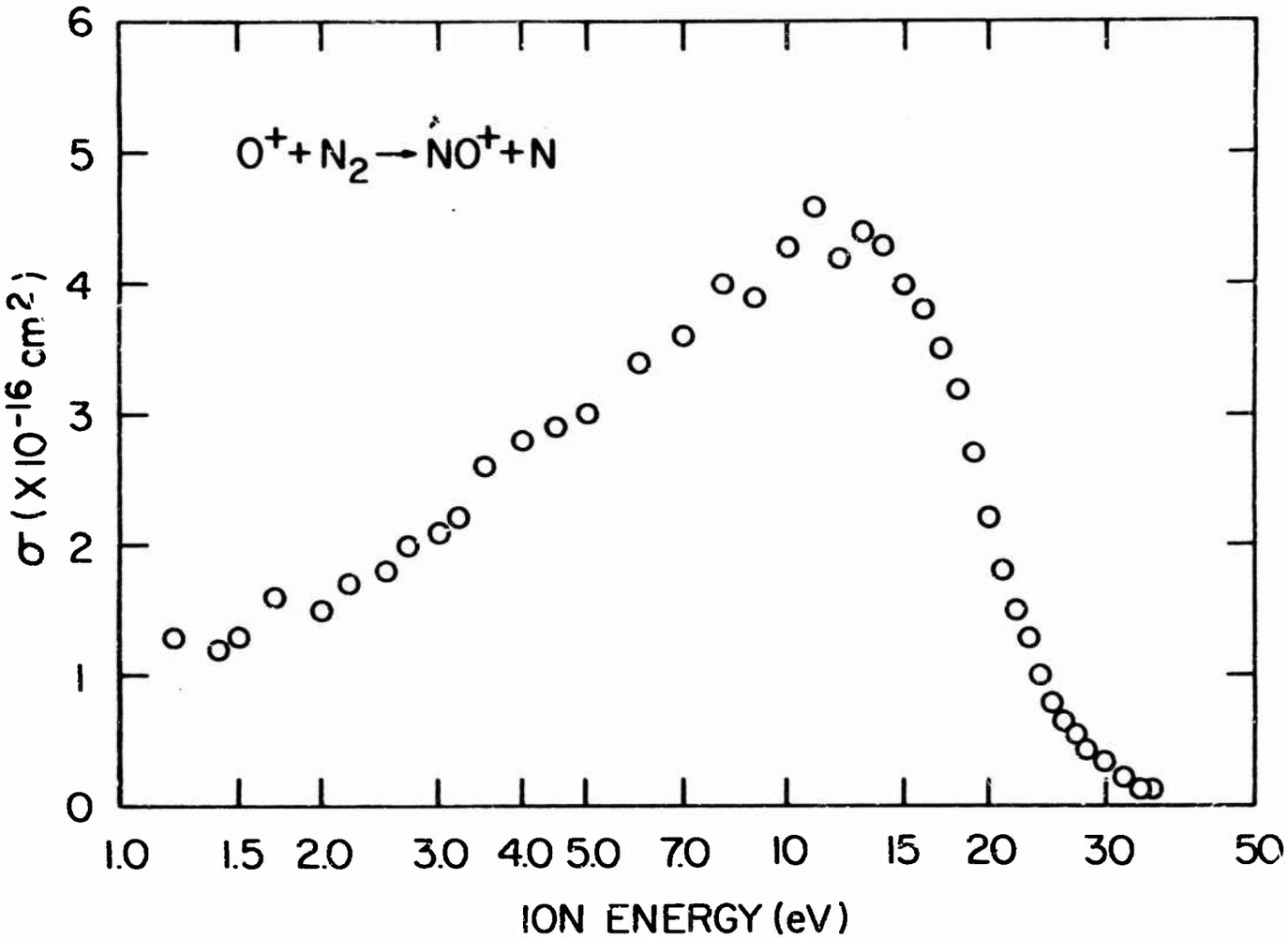

Fig. 11. Ion molecule reaction cross section for O^+ ions incident on neutral nitrogen molecules to form NO^+ as a function of the energy of the incident ion

REFERENCES

1. M. H. Bortner, Coordinator, DNA Reaction Rate Handbook, DASA-1948, General Electric Company Missile and Space Division, Philadelphia, Pennsylvania, 1967.

2. B. R. Turner and J. A. Rutherford, "Charge-Transfer and Ion-Atom Interchange Reactions of Water Vapor Ions," J. Geophys. Res. 73, 6751, 1968.

3. D. M. J. Compton and B. R. Turner, "Electronic and Ionic Reactions in Atmospheric Gases, Yearly Technical Summary Report, September 1, 1966, through August 31, 1967," DASA-1997, General Dynamics, General Atomic Division, October 27, 1967.

4. B. R. Turner, "Electronic and Ionic Reactions in Atmospheric Gases," Yearly Technical Summary Report, September 1, 1968, through November 30, 1968," DASA-2227, Gulf General Atomic, January 1, 1969.

5. B. R. Turner and J. A. Rutherford, "Electronic and Ionic Reactions in Atmospheric Gases, Yearly Technical Summary Report, December 1, 1968, through October 31, 1969," DASA-2398, Gulf General Atomic, January 28, 1970.

6. J. A. Rutherford, J. K. Layton, R. H. Neynaber, and D. A. Vroom, "Electronic and Ionic Reactions in Atmospheric Gases, Yearly Technical Summary Report, November 1, 1969, through August 31, 1970," DASA-2566, Gulf Radiation Technology, November 1970.

7. J. A. Rutherford, R. F. Mathis, B. R. Turner, and D. A. Vroom, "Formation of Magnesium Ions by Charge Transfer," accepted for publication by J. Chem. Phys.

8. R. F. Stebbings, B. R. Turner, and J. A. Rutherford, "Low-Energy Collisions Between Some Atmospheric Ions and Neutral Particles," J. Geophys. Res. 71, 771, 1966.

9. B. R. Turner, J. A. Rutherford, and R. F. Stebbings, "Charge Transfer Reactions of Nitric Oxide and Atomic and Molecular Ions of Oxygen and Nitrogen," J. Geophys. Res. 71, 4521, 1966.

10. C. F. Giese, "Strong Focusing Ion Source for Mass Spectrometers," Rev. Sci. Instr. 30, 260, 1959.

References (Cont.)

11. M. Knudsen, "Kinetic Theory of Gases," Methuen's Monographis on Physical Subjects, 3rd ed., London, Methuen & Co. Ltd., 1950.

12. F. A. Wolf and B. R. Turner, "Energy Dependence of the Charge-Transfer Reaction in Thermal and Low-Electron-Volt Region," J. Chem. Phys. 48, 4266, 1968.

13. D. Rapp and W. E. Francis, "Charge Exchange Between Gaseous Ions and Atoms," J. Chem. Phys. 37, 2631, 1962.

14. G. Gioumousis and D. P. Stevenson, "Reactions of Gaseous Molecule Ions with Gaseous Molecules; V. Theory," J. Chem. Phys. 29, 294, 1958.

15. R. S. Narcisi and A. D. Bailey, "Mass Spectrometric Measurements of Positive Ions at Altitudes from 64 to 112 Kilometers," J. Geophys. Res. 70, 3687, 1965.

16. W. Swider, Jr., "Processes for Meteoric Elements in the E-Regions," Planet. Space Sci. 17, 1233, 1969.

17. C. E. Moore, "Ionization Potentials and Ionization Limits Derived from the Analyses of Optical Spectra," National Standard Reference Data System NBS-34.

18. B. R. Turner, J. A. Rutherford, and D. M. J. Compton, "Abundance of Excited Ions in O^+ and O_2^+ Ion Beams," J. Chem. Phys. 48, 1602, 1968.

19. W. B. Maier and E. Murad, "A Study of Collisions Between Low-Energy N^+ and N_2: Reaction Cross Sections, Isotopic Compositions, and Kinetic Energies of the Products," Los Alamos Scientific Laboratory Report LA-DC-12542, March 1971.

20. K. P. Huber, "The Excited Electronic States of the NO^+ Ion," Canadian J. Phys. 46, 1691, 1968.

21. P. D. Goldan, A. L. Schmeltekopf, F. C. Fehsenfeld, H. I. Schiff, and E. E. Ferguson, "Thermal Energy Ion-Neutral Reaction Rates; II. Some Reactions of Ionospheric Interest," J. Chem. Phys. 44, 4095, 1966.

References (Cont.)

22. R. S. Mulliken, "Electronic Structures of Molecules; XIV. Linear Triatomic Molecules, Especially Carbon Dioxide," J. Chem. Phys. 3, 720, 1935.

23. J. J. Kaufman and W. S. Koski, "Theoretical Justification of the Apparently Anomalous Low-Energy Behavior of Some Ion-Molecule Reactions," J. Chem. Phys. 50, 1942, 1969.

24. C. F. Giese, "The Reaction $O^+ + N_2 \rightarrow NO^+ + M$," from "Ion-Molecule Reactions in the Gas Phase," R. F. Gould, ed., Americal Physical Society Publications, Washington, 1966.

25. A. L. Schmeltekopf, F. C. Fehsenfeld, G. I. Gilman, and E. E. Ferguson, "Reaction of Atomic Oxygen Ions with Vibrationally Excited Nitrogen Molecules," Planet. Space Sci. 15, 401, 1967.

26. A. L. Schmeltekopf, E. E. Ferguson, and F. C. Fehsenfeld, "Afterglow Studies of the Reactions He^+, $He(2^3S)$, and O^+ with Vibrationally Excited N_2," J. Chem. Phys. 48, 2966, 1968.

APPENDIX

THE EFFECT OF METASTABLE $O^+(^2D)$ ON REACTIONS OF O^+ WITH NITROGEN MOLECULES*

J. A. Rutherford and D. A. Vroom

Gulf Radiation Technology
A Division of Gulf Energy & Environmental Systems Company
San Diego, California 92112

ABSTRACT

Laboratory measurements indicate that the metastable ions of O^+ in reaction with N_2 in the low-energy range (14 eV) react to form principally N_2^+, while the ion molecule reaction to form NO^+ has a very small probability. The ground-state O^+ ion reacts mainly to form NO^+. The abundance of metastable $O^{+2}D$ ions was determined using the observation that $O^{+2}D + N_2$ has a small cross section for forming NO^+. The ion-energy dependences for both reactions were measured within the energy range 1.0 to 500 eV.

*Work supported by Defense Nuclear Agency under contract DASA01-69-C-0044.

The ion-molecule reaction most widely dealt with by aeronomists has been that involving O^+ in collision with N_2 to form NO^+. The effect of excited states of O^+ on the rate of this reaction has been open to question. Dalgarno[A1] has pointed out that, in the F region, $O^+(^2D)$ ions are lost principally by collisions with neutral O_2 and N_2. An indication that the excited states may not be of importance in the formation of NO^+ was reported by Stebbings et al.[A2] who noted there was little change in the cross section for $O^+ + N_2 \rightarrow NO^+ + N$ when excited states of O^+ ions were introduced into the beam. The results reported here will show that the cross section for the reaction involving the excited atomic ion ($O^+(^2D) + N_2 \rightarrow NO^+ + N$) is, in fact, very small. Furthermore, we will indicate that the principal channel for these reactants results in production of N_2^+ which is probably formed in the ($A^2\Pi_u$) state.

The apparatus employed for the cross-section measurements has been described previously.[A2, A3] In this instrument, the primary ions are formed in an electron bombardment ion source, the electron energy of which can be carefully controlled. These ions are extracted from the source, mass-analyzed, and accelerated or retarded to the desired energy. This ion beam then crosses a modulated neutral beam (modulated at 100 Hz), in this case N_2. The products of collisions between the ion and neutral beams are extracted along the direction of the primary ion beam, accelerated, focussed, and mass-analyzed in a second mass spectrometer. The selected ions are then detected using an electron multiplier coupled with lock-in amplifier techniques.

The neutral beam is formed by effusion from a room-temperature orifice and modulated by mechanical chopping. The neutral-beam density is determined by measuring the pressure in the neutral source with a differential pressure manometer and calculating the effusion from this source under known geometrical conditions.

The ratio of the metastable electronic states to the ground state can be varied by careful control of the energy of the ionizing electrons in the primary ion source. When the electron energy is below the threshold for excited-state formation, no excited states can be formed, and the resultant beam will be composed entirely of ground-state ions. As the ionizing electron energy is increased, metastable ions will appear in the beam.

Two reactions have been studied in detail here. These are:

$$O^+ + N_2 \rightarrow NO^+ + N \qquad \text{(A1)}$$

and

$$O^+ + N_2 \rightarrow O + N_2^+ . \qquad \text{(A2)}$$

The effects of metastable O^+ ions in the primary ion beam for Reaction 1 can be seen in Fig. A1. Here, the relative probability for forming NO^+ in collisions between O^+ and N_2 is plotted as a function of the electron energy used to form the O^+ ion. Two cases are shown: one in which pure oxygen is used in the ion source and the other in which the source contained 1% O_2 in pure helium. The latter case has been included since it gives an enhancement in the number of metastable O^+ ions in the beam and, therefore, better illustrates our conclusions. This enhancement arises because helium ions formed in the source will undergo a dissociative charge-transfer process with O_2 to yield the metastable $O^+(^2D)$. Note that the NO^+ data in Fig. A1 have been normalized to a value of 10 at 21 eV. This is below the threshold of 22 eV required for production of $O^+(^2D)$ from molecular oxygen if the formation of $O^+(^2D)$ from pair production is neglected. This latter process is known to have a small cross section. The

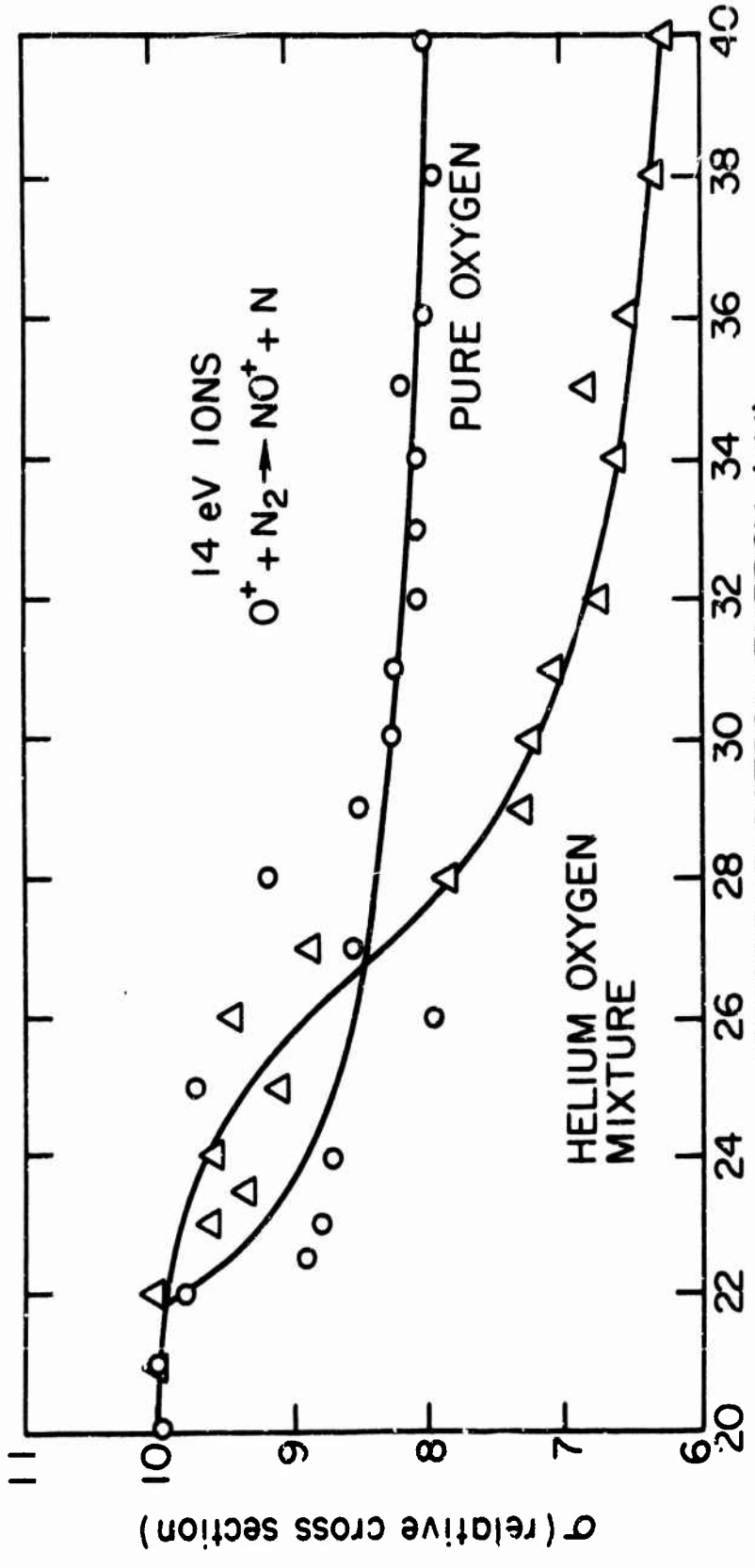

Fig. A1. Graphical representation of the decrease in the relative cross section for formation of NO^+ ions from O^+ impinging on N_2 as a function of the ion source electron energy. The ion neutral interaction energy is 14 eV. The open circles represent the case for pure O_2 in the source, while the open triangles represent the case for an O_2/He mixture.

curves show that for the formation of NO^+, the relative cross section normalized on the total O^+ current starts to decrease in the case of pure oxygen above the threshold for $O^+(^2D)$, indicating that the presence of this excited state depletes the number of ground-state particles available for reaction. This same result is seen for the helium/oxygen mixture, except that the effect is not seen until slightly higher in energy due to the excited state not being formed in significant concentration until above the ionization threshold for helium.

The electron-energy dependence for the reaction $O^+ + N_2 \rightarrow O + N_2^+$ is given in Fig. A2. The cross section shown in this figure (the observed cross section) is obtained using the total O^+ current. An effect opposite to that seen in Fig. A1 is observed here. In the curve for pure O_2, it is noted that the observed cross section for forming N_2^+ is very small for electron energies below the $O^+(^2D)$ threshold and then increases as the number of excited states is increased. The effect is the same for the oxygen-helium mixtures below the threshold for ionization of helium, but it more pronounced above this point as more excited states are then present. It must be noted that all the data shown in the figures are for a fixed ion-neutral interaction energy of 14 eV and illustrate the change which this cross section undergoes as the number of excited states in the beam is varied. An interaction energy of 14 eV was chosen because the ion-molecule cross-section curve peaks at this value.

Examination of the figures allows the following conclusions to be drawn.

$$O^+(^4S) + N_2 \rightarrow NO^+ + N\,, \tag{A3}$$

$$O^+(^4S) + N_2 \rightarrow O + N_2^+\,, \tag{A4}$$

$$O^+(^2D) + N_2 \rightarrow O + N_2^+\,. \tag{A5}$$

That is, Fig. A1 shows that NO^+ is formed below the threshold for excited O^+ ions (Reaction 3). Similarly, Fig. A2 shows that below the $O^+(^2D)$

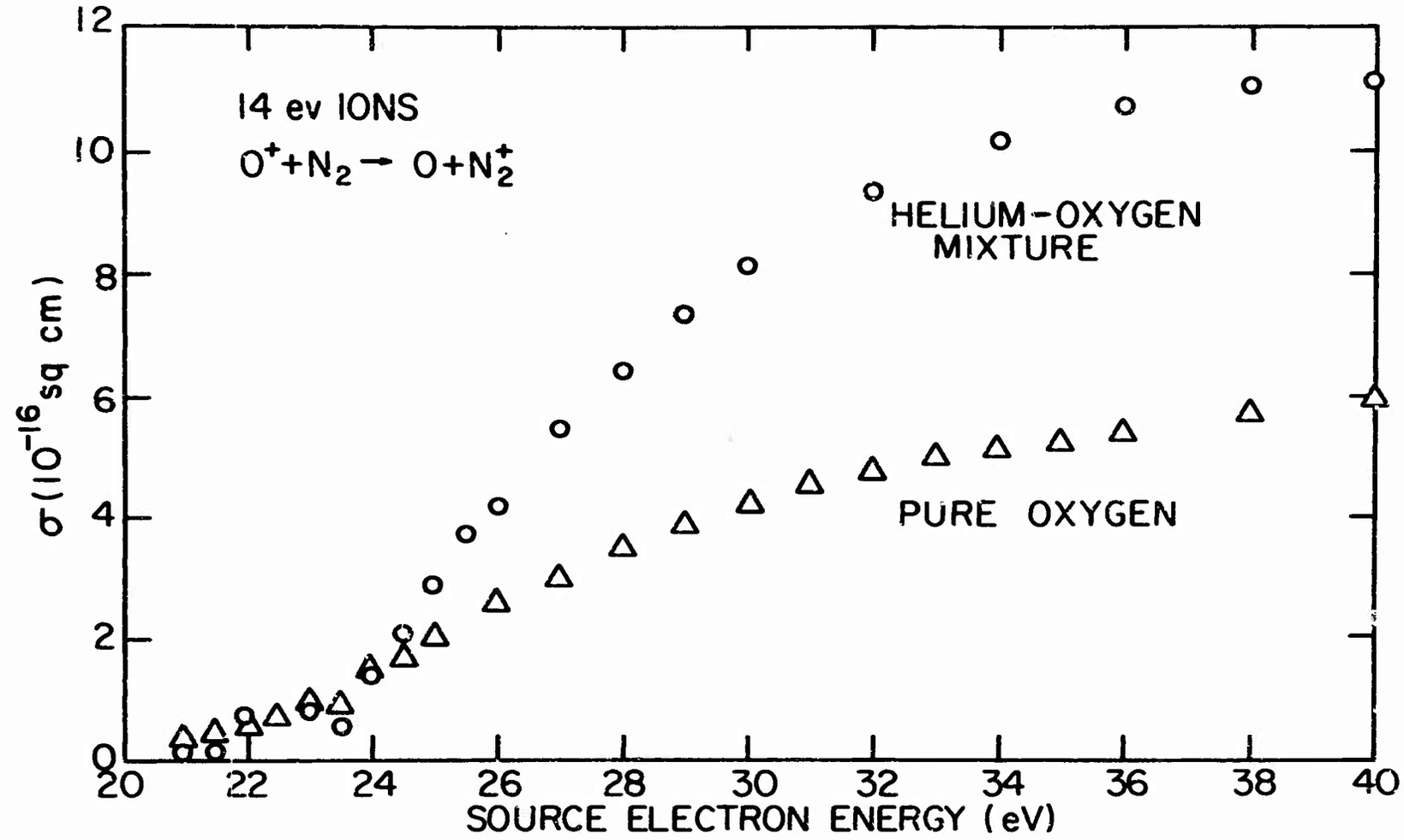

Fig. A2. Observed cross section for the charge-transfer reaction $O^+ + N_2 \rightarrow O + N_2^+$ as a function of the ion-source electron energy. The ion neutral interaction energy is 14 eV. The open circles represent the case for pure O_2 in the source, while the open triangles represent the case for an O_2/He mixture.

threshold, very little N_2^+ is formed (Reaction 4), but that above the onset of the excited state, N_2^+ is readily formed (Reaction 5). Using the above information coupled with previously obtained results, we will show that

$$O^+(^2D) + N_2 \rightarrow NO^+ + N . \tag{A6}$$

Assume that the cross section for this process is small compared to that for Reaction 3. Now, since the observed cross section σ for any process can be written as

$$\sigma = \sum_n \sigma_n f_n , \tag{A7}$$

where σ_n is the cross section for reactant ions in state n present in fractional abundance f_n, we can write our total cross section for formation of NO^+ as

$$\sigma = \sigma_{(^4S)} f_{(^4S)} + \sigma_{(^2D)} f_{(^2D)} . \tag{A8}$$

Since we have assumed that $\sigma_{(^2D)} << \sigma_{(^4S)}$, the presence of this species in the total O^+ beam can be shown to lower the observed cross section by a percentage equal to its fractional abundance. Examination of Fig. A1, therefore, reveals that for electrons of 40 eV, the excited state concentration is 20% of the total beam for pure O_2 and 37.5% for the oxygen/helium mixture. As discussed above, Fig. A2 shows that the charge-transfer process between O^+ ions and N_2 goes primarily with the excited state (Reactions 4 and 5). Using the fractional abundances determined above, it is, therefore, possible to correct the observed cross sections for Reaction 5 obtained using the total O^+ beam intensity. For Reaction 5 ($O^+(^2D) + N_2 \rightarrow O + N_2^+$) we get, for 14-eV ions colliding with the neutral particle, a cross section of 29.5×10^{-16} cm^2 for the pure O_2 case and a cross section of 30.6×10^{-16} cm^2 for the oxygen/helium mixture.

Using a totally different technique developed previously in this laboratory,[A4] we have determined the fractional abundance of $O^+(^2D)$ from the attenuation of an O^+ beam in another gas to be 24%. This value was obtained using 40-eV electron energy in pure O_2. Using this value for the fractional abundance, we have obtained a cross section for Reaction 5 at 14 eV of 26.8×10^{-16} cm^2. The difference between this value and those determined above is within experimental error and, therefore, indicates that our assumption of a small cross section for Reaction 6 is valid.

Using the fractional abundances determined above, it is possible to obtain cross-section curves for the separate ion states for each reaction that is found to proceed with large probability. The charge-exchange cross section leading to production of N_2^+ is given in Fig. A3. The values given by this figure are slightly lower at low energies than those reported previously.[A2] Cross sections for the ion molecule reaction producing NO^+ are given in Table A1.

Figure A3 shows that the cross section for the reaction of $O^+(^2D)$ with N_2 remains large down to the lowest interaction energy studied. The energy available in charge transfer with $O^+(^2D)$ is 16.1 eV. This energy is almost exactly that required for formation of the N_2^+ in the ($A^2\Pi_u$, v=1) state. This reaction is, therefore, a source of excited N_2^+ ions in the F region where the O^+ concentration is high. Decay of the $N_2^+(A^2\Pi_u)$ state produces Meinel radiation. A discussion of how this reaction may lead to an enhancement of the Meinel radiation observed from airglow has been given by Wallace and Broadfoot.[A5]

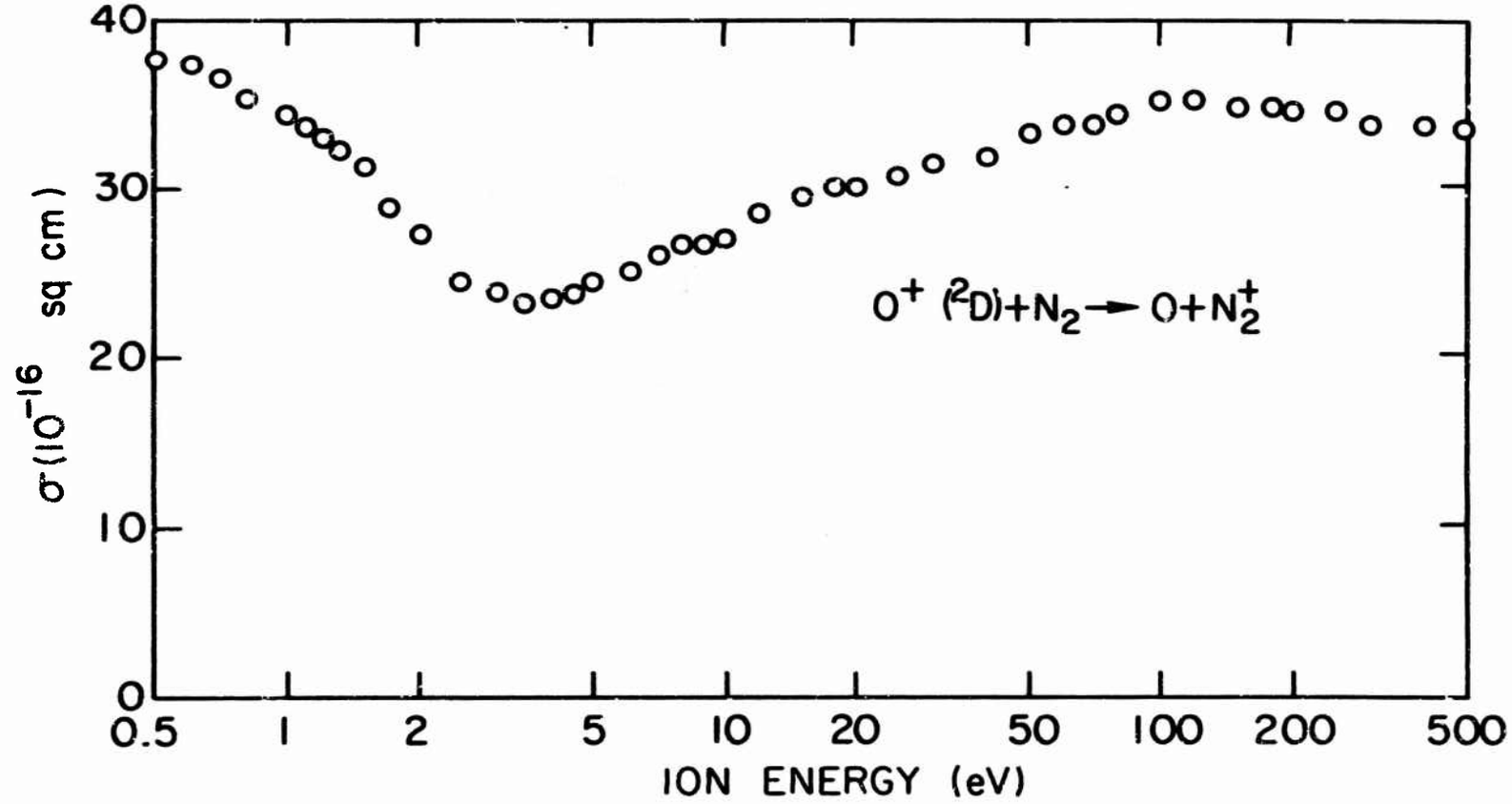

Fig. A3. Charge transfer cross section for $O^+(^2D) + N_2 - O + N_2^+$ as a function of the ion energy in the laboratory system

Table A1

CROSS SECTION FOR $O^+ + N_2 \rightarrow NO^+ + N$

Laboratory Energy (eV)	Center of Mass Kinetic Energy (eV)	Cross Section ($\times 10^{-16}$ cm^2)
1.2	0.76	1.3
1.4	0.89	1.2
1.5	0.95	1.3
1.7	1.08	1.6
2.0	1.27	1.5
2.2	1.40	1.7
2.5	1.59	1.8
2.7	1.72	2.0
3.0	1.91	2.1
3.2	2.04	2.2
3.5	2.23	2.6
4.0	2.55	2.8
4.5	2.86	2.9
5.0	3.18	3.0
6.0	3.82	3.4
7.0	4.45	3.6
8.0	5.09	4.0
9.0	5.73	3.8
10.0	6.36	4.3
11.0	7.00	4.6
12.0	7.64	4.2
13.0	8.27	4.4
14.0	8.91	4.3
15.0	9.55	4.0
16.0	10.18	3.8
17.0	10.82	3.5
18.0	11.45	3.2
19.0	12.09	2.7
20.0	12.73	2.2
21.0	13.36	1.8
22.0	14.00	1.5
23.0	14.64	1.3
24.0	15.27	1.0
25.0	15.91	0.80
26.0	16.55	0.65
27.0	17.18	0.53
28.0	17.82	0.44
30.0	19.09	0.34
32.0	20.36	0.22
34.0	21.64	0.15
35.0	22.27	0.15

REFERENCES

A1. A. Delgarno and M. B. McElroy, Planet. Space Sci. 11, 727, 1963.

A2. R. F. Stebbings, B. R. Turner, and J. A. Rutherford, J. Geophys. Res. 71, 771, 1966.

A3. J. A. Rutherford, R. F. Mathis, B. R. Turner, and D. A. Vroom, "Formation of Magnesium Ions by Charge Transfer," accepted for publication in J. Chem. Phys.

A4. B. R. Turner, J. A. Rutherford, and D. M. J. Compton, J. Chem. Phys. 48, 1602, 1968.

A5. L. Wallace and A. L. Broadfoot, Planet. Space Sci. 17, 975, 1969.